NASA TECHNICAL REPORT

NASA TR R-349

c.1

NASA TR R-349

DIFFUSION MODEL STUDY IN CHEMICALLY REACTING AIR COUETTE FLOW WITH HYDROGEN INJECTION

by Randolph A. Graves, Jr.

Langley Research Center
Hampton, Va. 23365

NATIONAL AERONAUTICS AND SPACE ADMINISTRATION • WASHINGTON, D. C. • OCTOBER 1970

1. Report No.	2. Government Accession No.	3. Recipient's Catalog No.
NASA TR R-349		

4. Title and Subtitle

DIFFUSION MODEL STUDY IN CHEMICALLY REACTING AIR COUETTE FLOW WITH HYDROGEN INJECTION

5. Report Date: October 1970

6. Performing Organization Code

7. Author(s)

Randolph A. Graves, Jr.

8. Performing Organization Report No.: L-6960

9. Performing Organization Name and Address

NASA Langley Research Center
Hampton, Va. 23365

10. Work Unit No.: 124-07-18-06

11. Contract or Grant No.

13. Type of Report and Period Covered: Technical Report

12. Sponsoring Agency Name and Address

National Aeronautics and Space Administration
Washington, D.C. 20546

14. Sponsoring Agency Code

15. Supplementary Notes: Part of the information presented herein was included in a thesis entitled "Chemically Reacting Couette Flow With Hydrogen Injection for Two Diffusion Models" submitted in partial fulfillment of the requirements for the degree of Master of Science in Mechanical Engineering, Virginia Polytechnic Institute, Blacksburg, Virginia, June 1969.

16. Abstract

An analytical study of the effects of hydrogen injection and chemical reaction on the flow properties of Couette flow has been conducted. Special emphasis was given to the diffusion model assumed for the calculations. Three diffusion models were chosen for the analysis: Fick's law (binary diffusion), multicomponent diffusion, and an approximation to the multicomponent diffusion. In the Fick's law model, three methods of obtaining the diffusion coefficient were also investigated.

Implicit finite-difference numerical solutions to the governing equations for Couette flow were obtained for the three diffusion models over a range of hydrogen injection rates. The results indicate that there are significant differences between the solutions for the diffusion models and these differences are manifested most in the concentration profiles and the wall heating rates.

17. Key Words (Suggested by Author(s))

Diffusion
Couette flow
Hydrogen injection
Chemical reaction

18. Distribution Statement

Unclassified – Unlimited

19. Security Classif. (of this report)	20. Security Classif. (of this page)	21. No. of Pages	22. Price*
Unclassified	Unclassified	51	$3.00

*For sale by the Clearinghouse for Federal Scientific and Technical Information
Springfield, Virginia 22151

DIFFUSION MODEL STUDY IN CHEMICALLY REACTING AIR COUETTE FLOW WITH HYDROGEN INJECTION[1]

By Randolph A. Graves, Jr.
Langley Research Center

SUMMARY

An analytical study of the effects of hydrogen injection and chemical reaction on the flow properties of Couette flow has been conducted. Special emphasis was given to the diffusion model assumed for the calculations. Three diffusion models were chosen for the analysis: Fick's law (binary diffusion), multicomponent diffusion, and an approximation to the multicomponent diffusion. In the Fick's law model, three methods of obtaining the diffusion coefficient were also investigated.

Implicit finite-difference numerical solutions to the governing equations for Couette flow were obtained for the three diffusion models over a range of hydrogen injection rates. The results indicate that there are significant differences between the solutions for the diffusion models and these differences are manifested most in the concentration profiles and the wall heating rates.

INTRODUCTION

The use of mass-transfer cooling to reduce aerodynamic heating encountered in reentry thermal environments has become widely accepted. Whether this mass-transfer cooling is accomplished by ablation or transpiration, the gases injected into the boundary layer are generally very different from those in the main stream flow. Since the convective heating reduction, as shown in reference 1, is greatest with low-molecular-weight gases, molecular hydrogen is usually a major component of the injected gases especially in the ablation of polymeric materials. The introduction of hydrogen into boundary-layer flow complicates the analysis because large property variations occur and molecular diffusion and chemical reactions must be considered.

---

[1]Part of the information presented herein was included in a thesis entitled "Chemically Reacting Couette Flow With Hydrogen Injection for Two Diffusion Models" submitted in partial fulfillment of the requirements for the degree of Master of Science in Mechanical Engineering, Virginia Polytechnic Institute, Blacksburg, Virginia, June 1969.

In most analyses, Fick's law (binary) diffusion (ref. 2) is assumed since it is a simple and easily applied approximation to the exact (thermal diffusion being neglected) but mathematically cumbersome Stefan-Maxwell multicomponent diffusion model (ref. 3). Recently, a third diffusion model, which is a more accurate approximation to the multicomponent diffusion model, has been proposed (ref. 3); this model utilizes a bifurcation of the binary diffusion coefficients to allow explicit solution of the Stefan-Maxwell relations for the diffusive fluxes. However, since both the Fick's law and bifurcation models are approximations, the calculated diffusion velocities may be in error, especially when there are large differences in the molecular weights of the diffusing species as is the case when hydrogen is present in an airstream. Thus, a comparison of the diffusion models is necessary to provide an estimate of the errors incurred in using the approximate models when low-molecular-weight gases diffuse through heavier gases.

There exists little information in the literature concerning the effects of the diffusion model on the solutions obtained for a chemically reacting airflow with hydrogen injection. There are no direct comparisons between the approximate diffusion models and the exact multicomponent diffusion model available from the literature. The analysis of Libby and Pierucci (ref. 4) does consider hydrogen injection into a laminar air boundary layer with variable properties, a chemical reaction, and multicomponent diffusion, but these solutions are compared with rather limited (Prandtl and Schmidt numbers equal to 1) solutions and give no insight into the effect of the diffusion model utilized. The present analysis differs from the analysis of reference 4 in that the approximate diffusion models employ the same assumptions as the multicomponent diffusion analysis, except for the diffusion model itself.

In making a comparison of the diffusion models, any simplification that can be used without concealing the important aspects of hydrogen injection into an air boundary layer is desirable. In the literature the one-dimensional Couette flow has been used as a simulation of the two-dimensional laminar boundary layer (refs. 5 and 6); however, the sources available consider only hydrogen injection into an air Couette flow with constant properties and no chemical reactions. The principal analysis is that of Eckert and Schneider (ref. 5), but because of their assumptions of no chemical reactions and incompressible Couette flow, their solutions are of limited usefulness. A variable property analysis is given in reference 6 where hydrogen is injected into a nitrogen stream, again with no chemical reactions and for binary diffusion only.

The present analysis differs from those of references 5 and 6 in that variable properties, a chemical reaction, and three diffusion models are considered. Also, the present analysis does not employ the flame-sheet approximation as did Libby and Pierucci to define combustion but instead a diffusion flame results from the solution of the governing equations.

The primary purpose of this study is to compare the results obtained from the use of the three diffusion models. Also, as a result of this study, the effects of variable transport and thermodynamic properties and a chemical reaction on Couette flow can be observed. Finally, the influence of various methods of evaluating the Fick's law diffusion coefficient can be observed.

As in the references cited, the one-dimensional Couette flow model is used as an approximation of the two-dimensional laminar boundary layer; however, it is recognized that under the conditions of the present analysis, this approximation is not accurate, but the Couette flow model does allow a vehicle by which the diffusion models can be compared. In this Couette flow representation, the velocity of the moving plate represents the free-stream velocity, whereas the distance between the plates simulates the boundary-layer thickness.

SYMBOLS

C_p	specific heat of gas mixture
$C_{p,i}$	specific heat of individual species
$\mathfrak{D}$	binary diffusion coefficient
D	Fick's law diffusion coefficient
$\overline{D}$	average diffusion coefficient
F_w	nondimensional shear stress at wall
f	diffusion factor
h	static enthalpy
K	mass fraction
K_p	equilibrium constant
M	molecular weight
M_m	mixture molecular weight

N	finite-difference station number
N_{Ma}	Mach number
N_t	total number of finite-difference stations
p	pressure
Q_w	heat-transfer rate into wall
q_w	nondimensional heat-transfer rate into wall
R	universal gas constant
Re_v	injection parameter of reference 6, $\rho v s \int_0^1 \frac{1}{\mu} d\eta$
s	distance between porous surfaces
T	temperature
T^*	nondimensional temperature for Lennard-Jones collision integral
U	dimensionless flow velocity
u	flow velocity
V	diffusion velocity
v	mass average velocity
X	mole fraction
y	coordinate normal to lower porous surface
Z	pseudo mass fraction (eq. (42d))
α	coordinate parameter of reference 6, $\int_0^\eta \frac{d\eta}{\mu}$

α_ϵ reference coordinate of reference 6, $\int_0^1 \frac{d\eta}{\mu}$

β_1 coefficient used in bifurcation diffusion model calculations (eq. (42b))

β_2 coefficient used in bifurcation diffusion model calculations (eq. (42c))

γ nondimensional coordinate of reference 6, $\frac{\alpha}{\alpha_\epsilon}$

δ nondimensional mass addition rate

ϵ/k maximum energy of attraction

ζ_{ik} number of atoms of element k in a molecule of species i

η nondimensional coordinate

θ nondimensional temperature

θ_1 nondimensional temperature of reference 6, $\frac{T - T_w}{T_\infty - T_w}$

λ total thermal conductivity

λ' translational thermal conductivity

λ'' internal thermal conductivity

μ viscosity

ν number of species (4)

ρ mass density

σ collision diameter

τ shear stress

$\Omega^{(1,1)^*}$ reduced collision integral for diffusion

ω species production rate

ϕ coefficient used in viscosity calculation (eq. (26))

ψ coefficient used in thermal conductivity calculation (eq. (29))

Subscripts:

i,j ith or jth species

k kth element

m gas mixture

o no injection

w wall (lower porous surface)

∞ free stream (upper porous surface)

ref reference condition

A tilde ~ over a symbol denotes an elemental.

ANALYSIS

Figure 1(a) shows the one-dimensional Couette flow model used in the present analysis and figure 1(b) gives the corresponding finite-difference representation. The lower porous surface, at $y = 0$, is stationary whereas the upper porous surface, at $y = s$, moves with a uniform velocity u_∞. The lower surface is at the temperature T_w and the upper surface at T_∞. The hydrogen gas, initially at temperature T_w, is injected uniformly and perpendicularly into the flow through the stationary surface, and is removed uniformly through the upper surface in concept only since the boundary conditions require that the hydrogen concentration be zero at the upper surface.

Equations of Motion for Couette Flow

By use of the assumptions of reference 6, the basic governing equations of motion for Couette flow can be reduced to the following forms:

Continuity:

$$\frac{d(\rho v)}{dy} = 0 \tag{1}$$

Momentum:

$$\rho v \frac{du}{dy} = \frac{d}{dy}\left(\mu \frac{du}{dy}\right) \tag{2}$$

Energy:

$$\rho v \frac{dh}{dy} = \frac{d}{dy}\left(\lambda \frac{dT}{dy}\right) + \mu\left(\frac{du}{dy}\right)^2 - \frac{d}{dy}\sum_i \rho_i V_i h_i \tag{3}$$

Species continuity:

$$\rho v \frac{dK_i}{dy} + \frac{d}{dy}(\rho_i V_i) = \omega_i \tag{4}$$

A simplification of the species continuity equations can be obtained through the introduction of the concept of elemental mass fractions as expressed by Lees in reference 7. The elemental mass fraction concept results from the fact that the mass of individual chemical elements is preserved in any chemical reaction not involving nuclear transformation. The elemental mass fraction is given by the expression:

$$\tilde{K}_k = \sum_i \zeta_{ik} \frac{M_k}{M_i} K_i \tag{5}$$

The elemental continuity equations can be obtained by multiplying equations (4) by $\zeta_{ik} \frac{M_k}{M_i}$ and summing over i, and, as a result, the elemental equations

$$\rho v \frac{d\tilde{K}_k}{dy} + \frac{d}{dy}\left(\sum_i \zeta_{ik} \frac{M_k}{M_i} \rho_i V_i\right) = 0 \tag{6}$$

are obtained. The introduction of the elemental mass fraction eliminates the species production terms ω_i of equations (4) and reduces the number of calculations to be made. There is now one equation of this form for each element as opposed to one equation of the form of equations (4) for each chemical species.

In the present analysis there will be three elements H, N, and O, and four chemical species O_2, H_2, N_2, and H_2O considered with one chemical reaction of the form:

$$H_2 + \frac{1}{2} O_2 \rightleftharpoons H_2O$$

This same chemical system was used by Libby and Pierucci in reference 4, and does not consider dissociation or ionization. The maximum gas temperature in the present study is less than 2400° K, and at this temperature and the pressure of 1 atmosphere assumed for this study, the amount of dissociation of O_2, H_2, and N_2 is negligible (1 atmosphere = 101.325 kN/m^2). The species considered have the necessary variation in molecular weight which is essential to the diffusion-model comparisons.

Boundary Conditions

At the moving surface (y = s), the following boundary conditions apply:

$$T = T_\infty$$

$$u = u_\infty$$

$$\tilde{K}_k = \tilde{K}_{k,\infty}$$

At the wall (y = 0), the boundary conditions are:

$$u = 0$$

$$T = T_w$$

The boundary conditions on the elemental mass fractions are derived as follows. Integration of the continuity equation (eq. (1)) yields

$$\rho v = \text{Constant} = (\rho v)_w$$

By using this relation, the elemental continuity equations can be integrated to give

$$\rho v \tilde{K}_k + \sum_i \zeta_{ik} \frac{M_k}{M_i} \rho_i V_i = \text{Constant} \tag{7}$$

The following subscript notation is adopted for the elements:

Element	Subscript
O	k = 1
H	k = 2
N	k = 3

By considering the injected hydrogen first, equations (7) become:

$$\tilde{\rho}_2 v + \tilde{\rho}_2 \tilde{V}_2 = \text{Constant}$$

$$\tilde{\rho}_2 (v + \tilde{V}_2) = \text{Constant}$$

$$\tilde{\rho}_2 \tilde{v}_2 = \text{Constant}$$

Evaluating the constant at the wall (y = 0) yields:

$$\tilde{\rho}_2\tilde{v}_2 = \left(\tilde{\rho}_2\tilde{v}_2\right)_w = (\rho v)_w$$

Thus, the wall boundary condition on the elemental hydrogen mass fraction becomes

$$(\rho v)_w \tilde{K}_{k,w} + \left(\sum_i \zeta_{ik} \frac{M_k}{M_i} \rho_i V_i\right)_w = (\rho v)_w \qquad (k = 2)$$

or

$$\tilde{K}_{k,w} = 1 - \frac{1}{(\rho v)_w}\left(\sum_i \frac{\zeta_{ik} M_k}{M_i} \rho_i V_i\right)_w \qquad (k = 2) \qquad (8)$$

A similar procedure is followed in evaluating the constant for the main stream elements where

$$\tilde{\rho}_1\tilde{v}_1 = \left(\tilde{\rho}_1\tilde{v}_1\right)_w = 0$$

$$\tilde{\rho}_3\tilde{v}_3 = \left(\tilde{\rho}_3\tilde{v}_3\right)_w = 0$$

The boundary conditions for these elements are:

$$\tilde{K}_{k,w} = -\frac{1}{(\rho v)_w}\left(\sum_i \zeta_{ik} \frac{M_k}{M_i} \rho_i V_i\right)_w \qquad (k = 1, 3) \qquad (9)$$

In order to simulate the two-dimensional boundary layer, the elemental mass fraction for hydrogen must approach zero at the upper boundary. This condition creates a correspondingly small elemental hydrogen density and since the elemental continuity equation $\tilde{\rho}\tilde{v}$ = Constant must be satisfied, the elemental transverse velocity becomes very large. This condition also introduces some uncertainty since the transverse velocity was assumed to be small in comparison with the main flow velocity to make possible the reduction of the general equations of motion. However, the inaccuracies incurred are confined to the region immediately adjacent to the upper boundary and are inherent in the use of the one-dimensional Couette flow to simulate the two-dimensional laminar boundary layer.

Nondimensional Form of the Governing Equations

The following new variables are introduced:

$$\eta = \frac{y}{s}$$

$$U = \frac{u}{u_\infty}$$

$$\theta = \frac{T}{T_\infty}$$

$$\delta = \frac{\rho v s}{\mu_\infty} = \frac{(\rho v)_w s}{\mu_\infty}$$

The governing equations in nondimensional form are:

Momentum:

$$\delta \frac{dU}{d\eta} = \frac{d}{d\eta}\left(\frac{\mu}{\mu_\infty}\frac{dU}{d\eta}\right) \tag{10}$$

Energy: (In addition to the nondimensional variables, the free-stream specific heat $C_{p,\infty}$ is needed to provide the following nondimensional energy equation.)

$$\frac{\delta}{C_{p,\infty}T_\infty}\frac{dh}{d\eta} = \frac{d}{d\eta}\left(\frac{\lambda}{C_{p,\infty}\mu_\infty}\frac{d\theta}{d\eta}\right) + \frac{u_\infty^2}{C_{p,\infty}T_\infty}\frac{\mu}{\mu_\infty}\left(\frac{dU}{d\eta}\right)^2 - \frac{d}{d\eta}\left(\sum_i \frac{\rho_i V_i s}{\mu_\infty}\frac{h_i}{C_{p,\infty}T_\infty}\right) \tag{11}$$

Elemental continuity:

$$\delta \frac{d\tilde{K}_k}{d\eta} = -\frac{d}{d\eta}\left(\sum_i \zeta_{ik}\frac{M_k}{M_i}\frac{\rho_i V_i s}{\mu_\infty}\right) \tag{12}$$

Nondimensional Boundary Conditions

The nondimensional boundary conditions at $\eta = 1$ are

$$U = 1$$

$$\theta = 1$$

$$\tilde{K}_k = \tilde{K}_{k,\infty}$$

At $\eta = 0$,

$$U = 0$$

$$\theta = \theta_w$$

$$\tilde{K}_{k,w} = 1 - \frac{1}{\delta}\left(\sum_i \zeta_{ik}\frac{M_k}{M_i}\frac{\rho_i V_i s}{\mu_\infty}\right)_w \qquad (k = 2) \tag{13}$$

$$\tilde{K}_{k,w} = -\frac{1}{\delta}\left(\sum_i \zeta_{ik}\frac{M_k}{M_i}\frac{\rho_i V_i s}{\mu_\infty}\right)_w \qquad (k = 1, 3) \tag{14}$$

Heat Transfer Into Wall

The heat-transfer rate into the wall is

$$Q_w = \left(\lambda_m \frac{dT}{dy} - \sum_i \rho_i V_i h_i \right)_w \tag{15}$$

Transformation of equation (15) yields

$$q_w = \frac{Q_w s}{\mu_\infty C_{p,\infty} T_\infty} = \left(\frac{\lambda_m}{\mu_\infty C_{p,\infty}} \frac{d\theta}{d\eta} - \sum_i \frac{\rho_i V_i s}{\mu_\infty} \frac{h_i}{C_{p,\infty} T_\infty} \right)_w \tag{16}$$

Shear Stress at Wall

The shear stress at the wall is

$$\tau_w = \mu_m \left. \frac{du}{dy} \right|_w \tag{17}$$

Transformation of equation (17) yields

$$F_w = \frac{\tau_w s}{u_\infty \mu_\infty} = \frac{\mu_m}{\mu_\infty} \left. \frac{dU}{d\eta} \right|_w \tag{18}$$

Gas Properties

The chemical thermodynamic and transport properties are calculated by the methods given in this section. The gas mixture is assumed to be at a pressure of one atmosphere for all calculations; however, comparison cases determined at lower pressures indicate only a minor influence of pressure on the solutions.

Chemical composition.- The following reaction is considered for the present analysis:

$$H_2 + \frac{1}{2} O_2 \rightleftharpoons H_2O$$

In addition, N_2 is present in the main Couette flow; thus, there are four chemical species to be considered in the equilibrium calculations. The equilibrium constant is related to the mole fractions by

$$K_p = p^{-1/2} \frac{X_{H_2O}}{X_{H_2} (X_{O_2})^{1/2}} \tag{19}$$

Substitution of

$$K_i = \frac{X_i M_i}{M_m} \tag{20}$$

into equation (5) yields

$$\tilde{K}_k = \frac{M_k}{M_m} \sum_{i=1}^{\nu} \zeta_{ik} X_i \qquad (k = 1, 2, 3) \tag{21}$$

The relation

$$\sum_{i=1}^{\nu} X_i = 1 \tag{22}$$

combined with equations (19) and (21) constitutes a system of five equations in the five unknowns, X_i (where $i = 1, 2, 3, 4$) and M_m. These equations were combined to eliminate four of the unknowns; one equation remained to be solved numerically for the mole fraction X_{O_2}. The equilibrium constant used in these calculations is taken from the JANAF tables (ref. 8). The species mass fractions are determined from the mole fractions by equation (20).

Thermodynamic properties.- The mixture density is obtained from the equation of state

$$\rho_m = \frac{pM_m}{RT} \tag{23}$$

and the enthalpy of the individual species is taken from the JANAF tables (ref. 8) and the mixture enthalpy is calculated by

$$h_m = \sum_{i=1}^{\nu} K_i h_i \tag{24}$$

Transport properties.- Rigorous kinetic theory expressions for the viscosity and thermal conductivity of gas mixtures have been developed and are presented by Hirschfelder, Curtiss, and Bird in reference 9, but these expressions are mathematically cumbersome. Somewhat simpler relations, which are approximations derived from the rigorous expressions, are given by Brokaw in reference 10 and are used in the present analysis. A comparison and discussion of approximate and rigorous expressions for an equilibrium reacting gas can be found in reference 11. In the present analysis the pure species viscosity and thermal conductivities are obtained from reference 12 where they were calculated by using the molecular constants given in table I and the Lennard-Jones (6-12) potential. (See ref. 9.)

The mixture viscosity is calculated from the pure component viscosities with the relation

$$\mu_m = \sum_{i=1}^{\nu} \frac{\mu_i}{1 + \sum_{\substack{j=1 \\ j \neq i}}^{\nu} \phi_{ij} \frac{X_j}{X_i}} \tag{25}$$

The coefficients ϕ_{ij} were derived in reference 10 by use of rigid-sphere theory and are a function of the pure component viscosities and molecular weight ratios

$$\phi_{ij} = \frac{\left[1 + \left(\frac{\mu_i}{\mu_j}\right)^{1/2} \left(\frac{M_j}{M_i}\right)^{1/4}\right]^2}{2\sqrt{2}\left(1 + \frac{M_i}{M_j}\right)^{1/2}} \tag{26}$$

The pure component viscosities are plotted in figure 2 where it is seen that hydrogen has a considerably lower viscosity than the remaining species.

The mixture thermal conductivity is obtained from the relation:

$$\lambda_m = \lambda'_m + \lambda''_m \tag{27}$$

The translational mixture conductivity is obtained from the pure component translational conductivities with the relation

$$\lambda'_m = \sum_{i=1}^{\nu} \frac{\lambda'_i}{1 + \sum_{\substack{j=1 \\ j \neq i}}^{\nu} \psi_{ij} \frac{X_j}{X_i}} \tag{28}$$

The coefficient ψ_{ij} is obtained from the viscosity coefficient ϕ_j by the following relationship obtained from reference 10:

$$\psi_{ij} = \phi_{ij}\left\{1 + 2.41\left[\frac{(M_i - M_j)(M_i - 0.142M_j)}{(M_i + M_j)^2}\right]\right\} \tag{29}$$

The internal mixture conductivity is obtained from the pure-component internal conductivities with the relation:

$$\lambda''_m = \sum_{i=1}^{\nu} \frac{\lambda''_i}{1 + \sum_{\substack{j=1 \\ j \neq i}}^{\nu} \phi_{ij} \frac{X_j}{X_i}} \tag{30}$$

The total thermal conductivity for each species is shown in figure 3 and as with the pure-component viscosities, the hydrogen is again very different from the remaining species, its thermal conductivity being much greater.

Diffusion Transport

The purpose of the present analysis is to compare solutions to the governing equations for Couette flow by using three different diffusion models: the approximate Fick's law diffusion model, the exact multicomponent diffusion model, and the bifurcation model. As will be seen below, the exact multicomponent diffusion model entails many mathematical operations and from a numerical analysis standpoint is not as desirable as the simpler but approximate Fick's law model. In the Fick's law diffusion model, three methods of calculating the diffusion coefficient are explored, the results indicating a wide variation in the solutions obtained.

Multicomponent diffusion.- The multicomponent diffusion fluxes were calculated by use of the Stefan-Maxwell relation from reference 9:

$$\frac{dX_i}{dy} = \sum_{\substack{j=1 \\ j\neq i}}^{\nu} \frac{X_i X_j}{\mathcal{D}_{ij}} \left(V_j - V_i\right) \tag{31}$$

and

$$\sum_{i=1}^{\nu} \rho_i V_i = 0 \tag{32}$$

Equation (31) can be rearranged to a more convenient form:

$$\frac{dX_i}{dy} = \sum_{\substack{j=1 \\ j\neq i}}^{\nu} \frac{X_i X_j}{\mathcal{D}_{ij}} - V_i \sum_{\substack{j=1 \\ j\neq i}}^{\nu} \frac{X_i X_j}{\mathcal{D}_{ij}} \tag{33}$$

Multiplying equation (33) by ρ/μ_∞ and introducing the nondimensional coordinates yields:

$$\frac{\rho}{\mu_\infty}\frac{dX_i}{d\eta} = \sum_{\substack{j=1 \\ j\neq i}}^{\nu} \frac{X_i X_j}{K_j \mathcal{D}_{ij}} \frac{\rho_j V_j s}{\mu_\infty} - \frac{\rho_i V_i s}{\mu_\infty} \sum_{\substack{j=1 \\ j\neq i}}^{\nu} \frac{X_i X_j}{K_i \mathcal{D}_{ij}} \tag{34}$$

Similarly, multiplying equation (32) by s/μ_∞ yields

$$\sum_{i=1} \frac{\rho_i V_i s}{\mu_\infty} = 0 \tag{35}$$

For the ν-species gas mixture, the diffusion fluxes $\rho_i V_i s/\mu_\infty$ are obtained from the simultaneous solution of $\nu - 1$ relations of the form of equation (34) and the relation given by equation (35).

The binary diffusion coefficients used in equation (34) are calculated by use of the following relation from reference 9:

$$\mathcal{D}_{ij} = 0.002628 \frac{\left[\frac{T^3(M_i + M_j)}{2M_iM_j}\right]^{1/2}}{p(\sigma_{ij})^2 \Omega_{ij}^{(1,1)^*}} \tag{36}$$

The collision cross section σ_{ij} is obtained from the relation

$$\sigma_{ij} = \frac{\sigma_i + \sigma_j}{2}$$

where the collision cross sections for each species are obtained from reference 12 and are given in table I.

The reduced collision integral $\Omega_{ij}^{(1,1)^*}$ is based on the Lennard-Jones (6-12) potential and is taken from reference 9 where it is tabulated as a function of the nondimensional temperature T_{ij}^* which is defined as

$$T_{ij}^* = \frac{T}{\epsilon_{ij}/k}$$

The maximum energy of attraction ϵ_{ij}/k in $^\circ K$ is obtained from

$$\frac{\epsilon_{ij}}{k} = \left(\frac{\epsilon_i}{k}\frac{\epsilon_j}{k}\right)^{1/2}$$

where the maximum energy of attraction for each species is taken from reference 12 and is given in table I. The binary diffusion coefficients obtained from equation (36) to be used in equation (34) are shown in figure 4, where it is apparent that the interactions involving the low-molecular-weight hydrogen produce larger binary diffusion coefficients.

Fick's law diffusion.- The Fick's law diffusion fluxes are calculated according to the following relation:

$$\rho_i V_i = -\rho D \frac{dK_i}{dy} \tag{37}$$

Knuth in reference 2 states that a sufficient condition for the applicability of equation (37) is that the binary diffusion coefficients are equal to each other and to the Fick's law diffusion coefficient. This assumption makes the Fick's law diffusion coefficient a pseudo binary diffusion coefficient and in the literature Fick's law diffusion is generally referred to as binary diffusion because of the appearance of equation (37). The term binary diffusion is adopted here for discussion purposes.

By multiplying equation (37) by $1/\mu_\infty$ and introducing the nondimensional coordinates, equation (37) becomes

$$\frac{\rho_i V_i s}{\mu_\infty} = -\frac{\rho D}{\mu_\infty}\frac{dK_i}{d\eta} \tag{38}$$

The calculation of the Fick's law diffusion coefficient can be accomplished in a number of ways; however, the following three methods have been selected for the present study.

Method 1: In the first method the diffusion coefficient is assumed to be independent of the molecular concentrations and is given by the self-diffusion relation from reference 9:

$$D = 0.002628\,\frac{\left(T^3/M\right)^{1/2}}{p\sigma^2\Omega^{(1,1)^*}} \tag{39}$$

where σ, M, and ϵ/k $\left(\text{needed to calculate } \Omega^{(1,1)^*}\right)$ are mixture averages as given in table I. Thus, D is dependent only on temperature and pressure. The diffusion coefficient calculated by equation (39) is given in figure 5. By comparison with figure 4, it is apparent that use of the average molecular constants causes the Fick's law diffusion coefficient to lie in the region of the heavy-molecule binary diffusion coefficients; thus, little of the effect of the low-molecular-weight hydrogen is provided.

Method 2: In the second method the diffusion coefficient is allowed some dependence on the molecular concentrations by allowing the molecular weight in equation (39) to vary as the mixture molecular weight. The diffusion coefficient is given by

$$D = 0.002628\,\frac{\left(T^3/M_m\right)^{1/2}}{p\sigma^2\Omega^{(1,1)^*}} \tag{40}$$

where σ and ϵ/k are given in table I. There is some inconsistency in using this procedure since the molecular weight is allowed to vary but not the other two molecular constants. However, the diffusion coefficient calculated by equation (40) does provide for a better representation of the average diffusion coefficient as seen in figure 5 where the diffusion coefficient covers a wide range of values more representative of the binary diffusion coefficients seen in figure 4. The upper and lower limits on the values seen in

figure 5 for equation (40) were determined by assuming that the stream consisted entirely of hydrogen (upper limit) and of air (lower limit).

Method 3: In the third method[2] the diffusion coefficient is a strong function of the molecular concentrations and is given by

$$D = 0.002628 \frac{(T^3)^{1/2}}{p} \sum_{i}^{\nu} \frac{X_i}{(M_i)^{1/2} \sigma_i^2 \Omega_i^{(1,1)^*}} \tag{41}$$

where σ_i, M_i, and ϵ_i/k are the molecular constants of the ith species and X_i is the mole fraction. Equation (41) provides the means of allowing the Fick's law diffusion coefficient for mixtures a wider variation of values than did either equation (39) or (40), as seen in figure 5. The upper and lower limits for equation (41) were determined in the same manner as the method 2 limits.

Bifurcation model.- The diffusion velocities are calculated by using the following simplified form of the Stefan-Maxwell relation (ref. 3):

$$\rho_i V_i = -\frac{\rho \bar{D}}{\beta_1} \left(\frac{\beta_2}{M_m} \frac{dZ_i}{dy} + \frac{Z_i - K_i}{M_m} \frac{d\beta_2}{dy} \right) \tag{42a}$$

where

$$\beta_1 = \sum_{i}^{\nu} X_i f_i \tag{42b}$$

$$\beta_2 = M_m \sum_{i}^{\nu} \frac{k_i}{f_i} \tag{42c}$$

$$Z_i = \frac{M_i X_i}{f_i \beta_2} \tag{42d}$$

$$\bar{D} = \frac{0.002628 \sqrt{T^3 / M_{ref}}}{p \sigma_{ref}^2 \Omega^{(1,1)^*}} \tag{43}$$

and the ν-diffusion factors f_i are obtained from a least-squares fit to the exact binary diffusion coefficients, to be described subsequently. Equation (42a) was obtained from the Stefan-Maxwell relation and equation (31) by a bifurcation of the binary diffusion coefficients,

[2]This method was suggested by Dennis O. Allison of the Langley Research Center.

$$\mathscr{D}_{ij} = \frac{\overline{D}}{f_i f_j} \tag{44}$$

where $\overline{D}$ is given by equation (43). The values for f are determined by finding the set of diffusion factors that gives the minimum total system residual error. Differentiating the total-system error relation

$$R = \sum_{i=1}^{\nu} \sum_{\substack{j=1 \\ j \neq i}}^{\nu} \left(\mathscr{D}_{ij} f_i f_j - \overline{D} \right)^2 \tag{45}$$

with respect to f and setting the resultant expression equal to zero yields

$$f_i = \frac{\overline{D} \sum_{\substack{j=1 \\ j \neq i}}^{\nu} \mathscr{D}_{ij} f_j}{\sum_{\substack{j=1 \\ j \neq i}}^{\nu} \mathscr{D}_{ij}^2 f_j^2} \tag{46}$$

from which the diffusion factors can be found by iteration. The diffusion factors are thus obtained from a least-squares fit to the kinetic-theory binary diffusion coefficients (eq. (36)). It is shown in reference 13 that the diffusion factors have only a weak dependence on temperature. In the present analysis, the f_i are assumed to be constant at the values given in table II and $\overline{D}$ has been evaluated by using the values for O_2 from table I for the reference constants. Table II also gives a comparison of the binary diffusion coefficients calculated by equations (36) and (44) where it is seen that equation (44) is a good approximation to the exact equation (eq. (36)); thus, the approximate bifurcation method should represent the exact multicomponent diffusion model fairly accurately.

The final form of the bifurcation diffusion flux relation is found by multiplying equation (42a) by $1/\mu_\infty$ and introducing the nondimensional coordinates to get

$$\frac{\rho_i V_i s}{\mu_\infty} = -\frac{\rho \overline{D}}{\beta_1 \mu_\infty} \left(\frac{\beta_2}{M_m} \frac{dZ_i}{d\eta} + \frac{Z_i - K_i}{M_m} \frac{d\beta_2}{d\eta} \right) \tag{47}$$

This equation is from a numerical standpoint easier to evaluate than the system of equations required by the multicomponent model (eqs. (34) and (35)).

Computation

The governing equations for Couette flow with hydrogen injection can be put in more convenient forms for numerical solution. Equation (10) is integrated and the constant of integration is evaluated at $\eta = 0$. The resulting momentum equation is

$$\frac{\mu_m}{\mu_\infty}\frac{dU}{d\eta} - \left(\frac{\mu_m}{\mu_\infty}\frac{dU}{d\eta}\right)_w = \delta U \tag{48}$$

Similarly, equation (11) is integrated and the constant of integration is evaluated at $\eta = 0$. The resulting energy equation is

$$\frac{\lambda_m}{C_{p,\infty}\mu_\infty}\frac{d\theta}{d\eta} - \left(\frac{\lambda_m}{C_{p,\infty}\mu_\infty}\frac{d\theta}{d\eta}\right)_w = \frac{\delta}{C_{p,\infty}T_\infty}\left(h_m - h_{m,w}\right) + \sum_i \frac{\rho_i V_i s}{\mu_\infty}\frac{h_i}{C_{p,\infty}T_\infty}$$

$$- \left(\sum_i \frac{\rho_i V_i s}{\mu_\infty}\frac{h_i}{C_{p,\infty}T_\infty}\right)_w - \int_0^\eta \frac{u_\infty^2}{C_{p,\infty}T_\infty}\frac{\mu_m}{\mu_\infty}\left(\frac{dU}{d\eta}\right)^2 d\eta \tag{49}$$

The solutions to the momentum and energy equations for all diffusion models are obtained by an implicit finite-difference numerical technique. Briefly, this technique involves expressing the derivatives on the left-hand side of each equation as four-point numerical differences and evaluating the right-hand side at each finite-difference station. The resulting system of linear algebraic equations is expressed in matrix form and a solution obtained therefrom.

The solution to the elemental continuity equation follows a somewhat similar procedure. Equation (13) is integrated and the constant of integration is evaluated at $\eta = 0$. The elemental continuity equation becomes

$$\tilde{K}_k = -\frac{1}{\delta}\sum_{i=1}^{\nu}\frac{\zeta_{ik}M_k}{M_i}\frac{\rho_i V_i s}{\mu_\infty} \qquad (k = 1, 3) \tag{50}$$

Since there are three elements in the system, only two elemental continuity equations need to be solved since the sum of the elemental mass fractions equals unity. For the multicomponent and bifurcation diffusion model solutions, equation (50) is solved by the method of successive approximations since the diffusion fluxes $\rho_i V_i s/\mu_\infty$ are given by equations (34), (35), and (47) from which the elemental profile dependence cannot be separated. In the case of the Fick's law solutions, the right-hand side of equation (50) can be partially replaced by equation (38) and by noting the definition of elemental mass fractions (eq. (5)), the following elemental continuity equation results:

$$\delta\tilde{K}_k - \frac{\rho D}{\mu_\infty}\frac{d\tilde{K}_k}{d\eta} = 0 \qquad (k = 1, 3) \tag{51}$$

In this simplified form, the elemental continuity equation for the binary diffusion model can be solved by use of the same implicit finite-difference scheme that was used to obtain solutions to the momentum and energy equations. The iterative solution of the finite-difference forms of the governing equations is accomplished by the iteration scheme given in reference 14.

RESULTS AND DISCUSSION

The results from a test case solved by the present numerical solution technique have been compared with the results from references 6 and 14. The flow problem is that of hydrogen injection into a nitrogen Couette flow for the following conditions: $T_\infty = 218^\circ$ K; $N_{Ma} = 12$; $T_w = 872^\circ$ K; and $Re_v = 0.5$. In each case the solutions were obtained with the assumption of variable properties and exact binary diffusion. As shown in figures 6 and 7, good agreement was obtained between the methods. This comparison case contains all the essential features of the present solution technique except for the chemical reaction itself; hence, the present numerical technique is thought to be sufficiently accurate to carry out the present investigation.

The remaining cases in this report consider the problem of hydrogen injection into air Couette flow. The values $T_\infty = 218^\circ$ K; $N_{Ma} = 6$; and $T_w = 872^\circ$ K were held constant for these cases. The influence of hydrogen injection was studied by allowing δ to assume the values $\delta = 0, 0.05, 0.1, 0.13, 0.2, 0.35, 0.5, 0.75, 1.0$, and 1.3. In the numerical calculations the solution for $\delta = 0$ (no injection) was obtained with 40 finite-difference stations; solutions for $\delta > 0$ were obtained with 50 finite-difference stations.

The no-injection temperature and velocity profiles are given in figure 8. It should be noted that the stream temperature increases only slightly above the wall value; thus, for the present conditions, the wall temperature is less than but close to the adiabatic wall temperature. The velocity profile is not a linear profile because of the viscosity variation through the stream.

Effect of Concentration Profiles on Transport Properties

The differences between the diffusion models are best seen in the concentration profiles in figure 9. It can be seen that changing δ produces changes in both the relative amounts of the various species and also produces variations in the profile shape. The biggest concentration differences occur for hydrogen, the wall concentration best reflecting this difference. This effect is summarized in figure 10 which gives the hydrogen concentration at the wall for all the diffusion models. It is readily seen that the binary diffusion model concentrations are much larger than the corresponding multicomponent and bifurcation models concentrations for all values of $\delta > 0.16$.

The concentration profiles determined by the three methods of evaluating the Fick's law diffusion coefficient show large variations in both magnitude and shape. In particular, the location of the flame zone is strongly dependent on the diffusion coefficient, the zone location moving away from the wall with increasing diffusion coefficient.

In general, figure 9 shows that there is little detectable difference between the multicomponent and the bifurcation models. This result would be expected from the comparison of binary diffusion coefficients given in table II. These figures also show that the method 3 binary model solutions, which are strongly concentration dependent, appear to give the best Fick's law solutions. This statement is especially true in the wall region which is most important for heat-transfer and shear-stress calculations.

The concentration differences seen in figure 9 alter the mixture transport properties at the wall, because hydrogen has a larger thermal conductivity and lower viscosity than the other species. This alteration of the transport properties is readily seen in figure 11 which gives a comparison of the mixture viscosity and thermal conductivity at the wall for the diffusion models. The greater hydrogen concentration of the binary diffusion model with methods 1 and 2 diffusion coefficients results in a mixture viscosity which is lower and a thermal conductivity which is higher than the other models. As would be expected from figure 10, there is no detectable transport-property difference between the multicomponent and bifurcation diffusion model solutions.

Temperature profiles.- The nondimensional temperature profiles are given in figure 12. The bifurcation and multicomponent diffusion models yield essentially identical results for the temperature profiles over all injection rates. The results for the binary model solutions show only fair to poor agreement with the multicomponent profiles, and the method 1 binary model solutions generally give the poorest agreement.

As an additional point of interest, the rather strong effect of the chemical reaction is seen by comparing the no-injection temperature profile of figure 8 with those of figure 12. The increase in peak stream temperature over the no-injection case approaches a factor of three at the higher injection rates.

Wall heating rates.- The wall-heating-rate curves shown in figure 13 point out some of the largest differences between the diffusion model results. The heating rates for the binary model are larger than the corresponding multicomponent and bifurcation models, the multicomponent and bifurcation models giving essentially identical results.

The heating rates due to conduction for the binary diffusion model with methods 1 and 2 diffusion coefficients are generally much larger than the corresponding multicomponent solutions whereas the heating rates due to diffusion (generally negative; energy diffusion away from lower surface) for the multicomponent and bifurcation diffusion models are larger because of the greater hydrogen diffusion velocity, the net effect being the lower heating rates for the multicomponent and bifurcation models.

Velocity profiles. The nondimensional velocity profiles are given in figure 14. There does not appear to be any major difference between the solutions for the diffusion models, especially at the lower injection rates where the amount of hydrogen and water are substantially reduced in comparison with the oxygen and nitrogen. Again, as in the case of the temperature profiles, the bifurcation and multicomponent diffusion models yield essentially identical results; however, the method 3 binary model solutions are also very close to those for the multicomponent and bifurcation models.

Shear stress.- The shear stress for the multicomponent and bifurcation diffusion models is higher than the corresponding binary diffusion model solutions for all injection rates. (See fig. 15.) This shear-stress difference results primarily from the mixture viscosity variations between the diffusion models. The pure component viscosities for hydrogen and water are lower than those for nitrogen and oxygen; as a result, mixture viscosity decreases with increasing hydrogen and water concentrations as seen in figure 11. This decreased mixture viscosity for the binary diffusion model causes the somewhat reduced shear stress as seen in figure 15. The method 3 shear stress is not as close to the multicomponent solution as might be expected.

Diffusion Coefficient Methods

The temperature and concentration dependences of the diffusion coefficients of the three binary methods were investigated. A single set of concentrations and temperatures was provided by the multicomponent solutions at an injection rate $\delta = 1.3$ for which there is a great deal of hydrogen present in the wall region.

In figure 16(a) it is apparent that the concentration dependence of the method 3 diffusion coefficient far outweighs its temperature dependence and also causes it to be much larger than the corresponding diffusion coefficients for methods 1 and 2. This larger diffusion coefficient in the wall region is responsible for the better comparisons of method 3 with the multicomponent solutions. A second multicomponent case was selected ($\delta = 0.13$) in which the hydrogen concentration was much less than that for the previous case. The diffusion coefficients for the three methods are plotted in figure 16(b).

Here it is seen that the method 3 diffusion coefficient is smaller than those for the other two methods and has the same temperature-dependent shape as these other methods. Figure 16(b) compared with figure 16(a) illustrates the strong effect of the hydrogen on the method 3 diffusion coefficients. The wider range of values given by the strong concentration dependence of the method 3 binary diffusion coefficients is responsible for the generally better comparisons with the multicomponent diffusion model solutions.

CONCLUDING REMARKS

A numerical study of the influence of various diffusion models on air Couette flow with hydrogen injection has been conducted. For this study the flow parameters were fixed with the moving wall temperature equal to 218° K, the moving wall Mach number equal to 6, and the stationary wall temperature equal to 872° K. The dimensionless injection rate was varied between zero and 1.3. Three diffusion models were included in the study: the Stefan-Maxwell multicomponent diffusion model, the bifurcation model (an approximation to multicomponent diffusion), and the Fick's law (binary diffusion) model. In addition, three variations on the method of calculating the Fick's law diffusion coefficient were investigated.

The results of the present investigation show that the bifurcation model yielded essentially the same results as the multicomponent diffusion model whereas the Fick's law model produced results for which the agreement with the multicomponent model ranged from very poor to fair. The best Fick's law results were obtained with a diffusion coefficient that was strongly concentration dependent. It was also found that for low injection rates, the calculated heating rates and shear stresses are not influenced by the diffusion model, but at high injection rates, these parameters are materially influenced by the increased hydrogen in the airstream.

The choice of a diffusion model for a particular problem obviously depends on the requirements for accuracy and ease of computation. The present case, involving hydrogen injection into air, provides a severe test for the two approximate diffusion models studied. The results have demonstrated that when properly applied, the Fick's law and bifurcation models can provide a fair degree of accuracy at significant savings in numerical complexity. It must be concluded that unless stringent requirements are placed on the accuracy of the results, one of the approximate models should be used. It must also be concluded that even when a high degree of accuracy is required, the bifurcation model should be investigated before resorting to the numerical complexities of the multicomponent diffusion model.

Langley Research Center,
National Aeronautics and Space Administration,
Hampton, Va., August 11, 1970.

REFERENCES

1. Gross, J. F.; Hartnett, J. P.; Masson, D. J.; and Gazley, Carl, Jr.: A Review of Binary Laminar Boundary Layer Characteristics. Int. J. Heat Mass Transfer, vol. 3, no. 3, Oct. 1961, pp. 198-221.

2. Knuth, Eldon L.: Multicomponent Diffusion and Fick's Law. Phys. Fluids, vol. 2, no. 3, May-June 1959, pp. 339-340.

3. Bartlett, Eugene P.; Kendall, Robert M.; and Rindal, Roald A.: An Analysis of the Coupled Chemically Reacting Boundary Layer and Charring Ablator. Part IV – A Unified Approximation for Mixture Transport Properties for Multicomponent Boundary-Layer Applications. NASA CR-1063, 1968.

4. Libby, Paul A.; and Pierucci, Mauro: Laminar Boundary Layer With Hydrogen Injection Including Multicomponent Diffusion. AIAA J., vol. 2, no. 12, Dec. 1964, pp. 2118-2126.

5. Eckert, E. R. G.; and Schneider, P. J.: Mass-Transfer Cooling in High-Speed Laminar Couette Flow. Tech. Rep. No. 12, Inst. Technol., Univ. Minnesota. Apr. 1957.

6. Simon, H. A.; Liu, C. S.; Hartnett, J. P.; and Chang, C. L.: Binary Couette Flow With Hydrogen Injection Into Carbon Dioxide and Nitrogen Streams. NASA CR-58497, 1964.

7. Lees, Lester: Convective Heat Transfer With Mass Addition and Chemical Reactions. Combustion and Propulsion – Third AGARD Colloquim, M. W. Thring, O. Lutz, J. Fabri, and A. H. Lefebvre, eds., Pergamon Press, 1958, pp. 451-498.

8. Anon.: JANAF Thermochemical Tables. Contract No. AF33(616)-6149, Thermal Lab., Dow Chem. Co., June 30, 1962.

9. Hirschfelder, Joseph O.; Curtiss, Charles F.; Bird, R. Byron: Molecular Theory of Gases and Liquids. John Wiley & Sons, Inc., c.1954. (Reprinted with corrections 1964.)

10. Brokaw, R. S.: Energy Transport in High Temperature and Reacting Gases. Planetary Space Sci., vol. 3, Feb. 1961, pp. 238-252.

11. Lee, Jerry S.; and Bobbitt, Percy J.: Transport Properties at High Temperatures of CO_2-N_2-O_2-Ar Gas Mixtures for Planetary Entry Applications. NASA TN D-5476, 1969.

12. Svehla, Roger A.: Estimated Viscosities and Thermal Conductivities of Gases at High Temperatures. NASA TR R-132, 1962.

13. Deblaye, Christian, and Bartlett, Eugene P.: An Evaluation of Thermodynamic and Transport Properties for Use in the Blimp Nonsimilar Multicomponent Boundary-Layer Program. Rep. No. 69-53, Aerotherm Corp., July 15, 1969.

14. Graves, Randolph A., Jr.: Chemically Reacting Couette Flow With Hydrogen Injection for Two Diffusion Models. M.S. Thesis, Virginia Polytech. Inst., 1969.

TABLE I.- MOLECULAR CONSTANTS

Species	ϵ/k, ^{o}K	σ, Å	M, g/g-mole
O_2	106.7	3.467	32.00
H_2	59.7	2.827	2.016
H_2O	809.1	2.641	18.02
N_2	71.4	3.798	28.02
Mixture	138.503	3.183	20.014

TABLE II.- COMPARISON OF BINARY DIFFUSION COEFFICIENTS AS COMPUTED BY THE BIFURCATION TECHNIQUE AND FROM KINETIC THEORY

[T = 1000° K]

Species		$\mathfrak{D}_{ij}$ (eq. (36)), cm^2/sec	f_i	$\mathfrak{D}_{ij}$ (eq. (44)), cm^2/sec	Percent error
i	j				
O_2	H_2	6.0174	0.97644	5.9018	-1.92
O_2	H_2O	2.0200		2.0140	-.29
O_2	N_2	1.5863		1.6249	2.44
H_2	H_2O	6.7932	.28259	6.9589	2.44
H_2	N_2	5.6324		5.6147	-.31
H_2O	N_2	1.9539	.82811	1.9160	-1.94
N_2			1.02636		

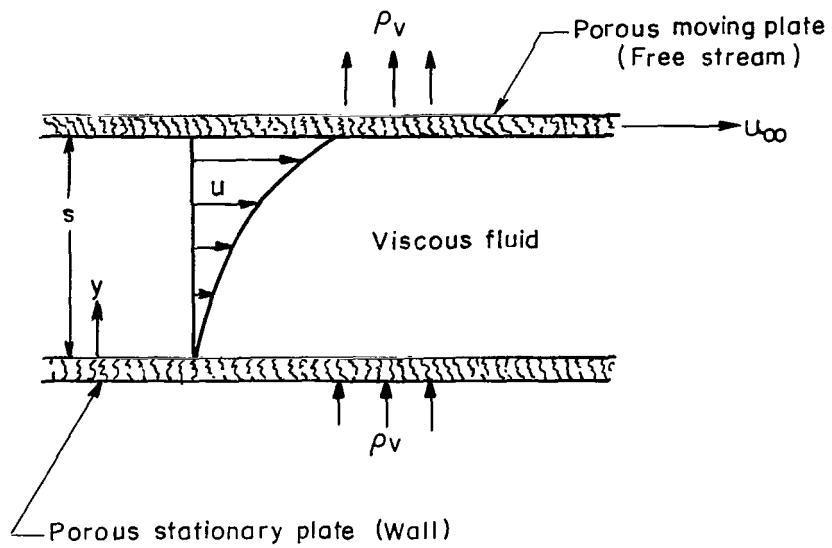

(a) Schematic diagram.

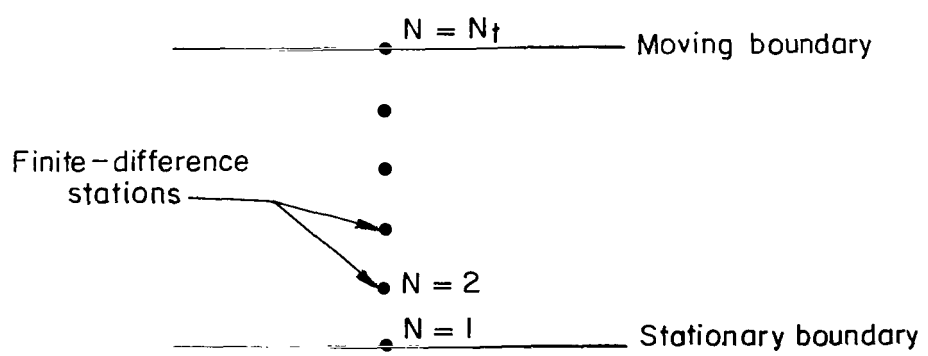

(b) Finite-difference representation.

Figure 1.- Couette flow model.

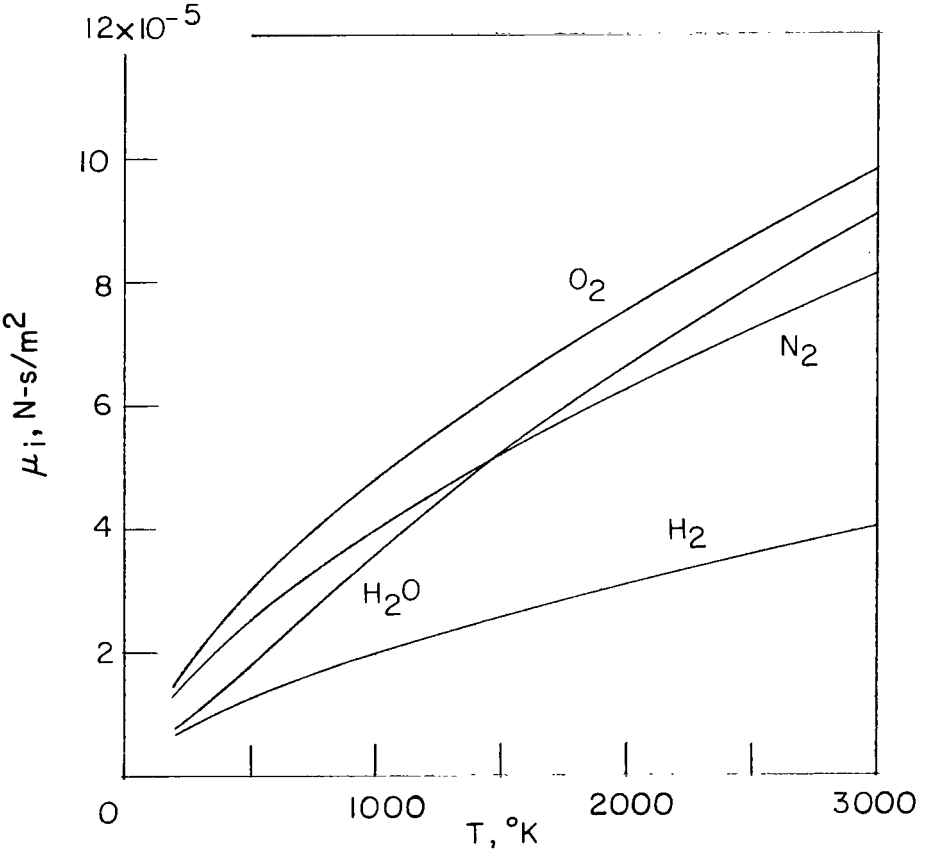

Figure 2.- Pure component viscosity.

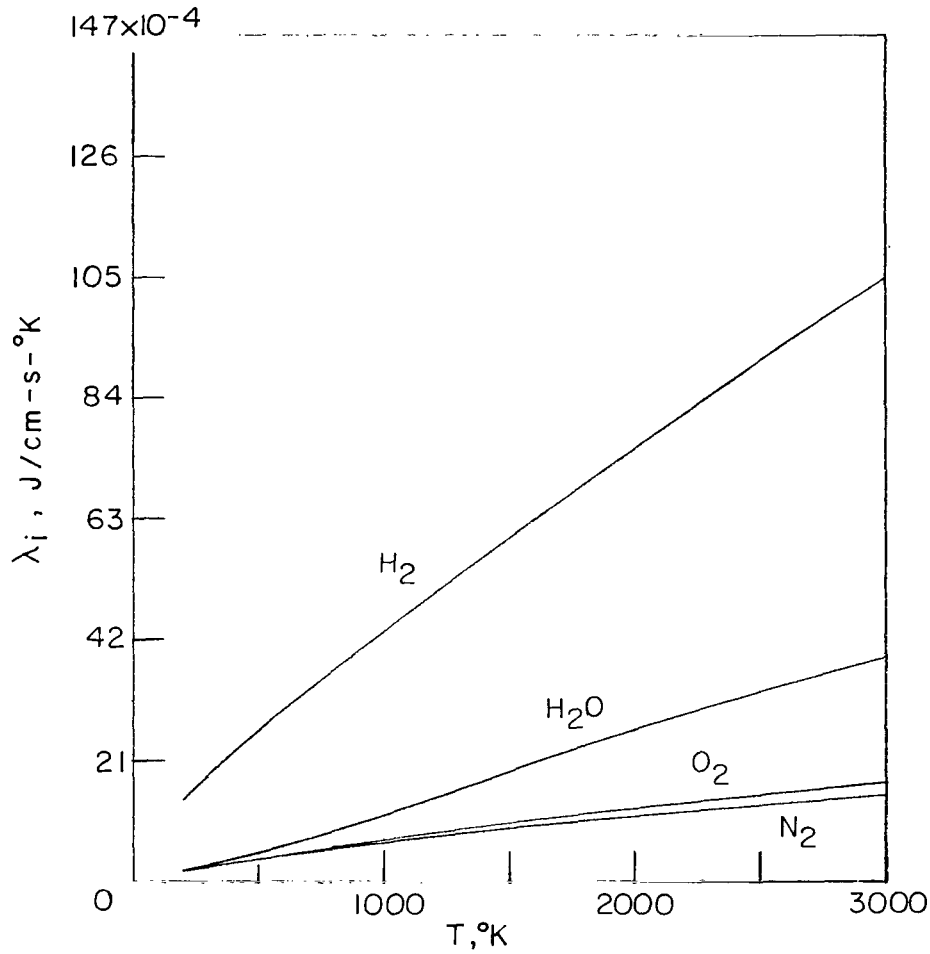

Figure 3.- Pure component total thermal conductivities.

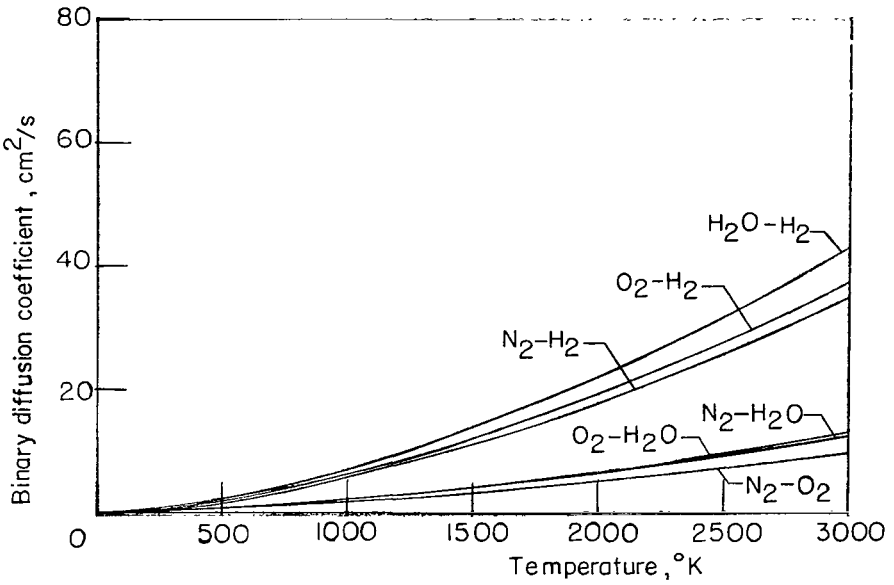

Figure 4.- Binary diffusion coefficients.

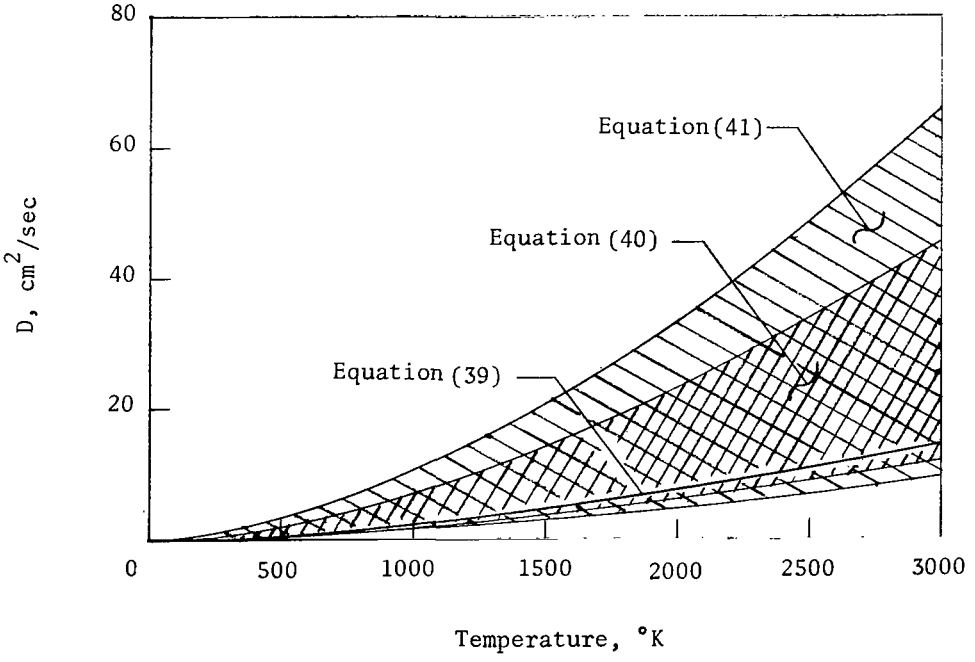

Figure 5.- Fick's law diffusion coefficients.

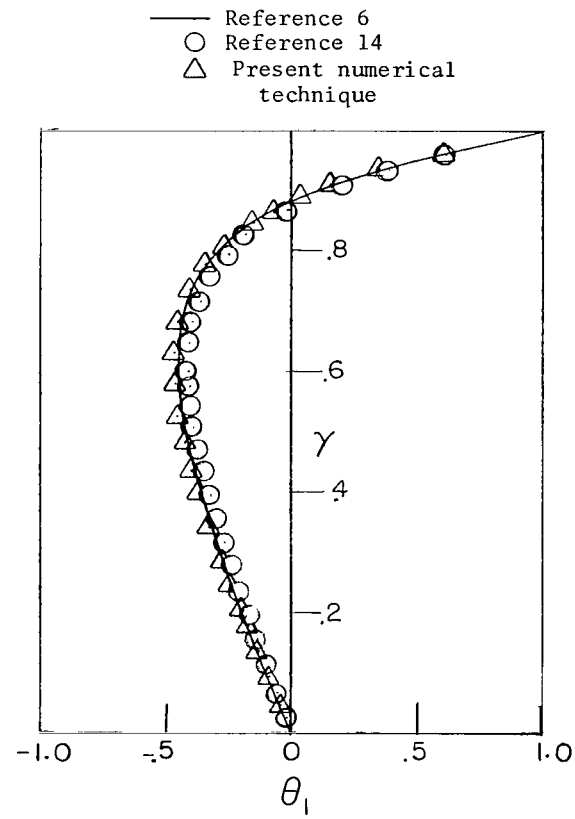

Figure 6.- Temperature profiles for nitrogen Couette flow with hydrogen injection.

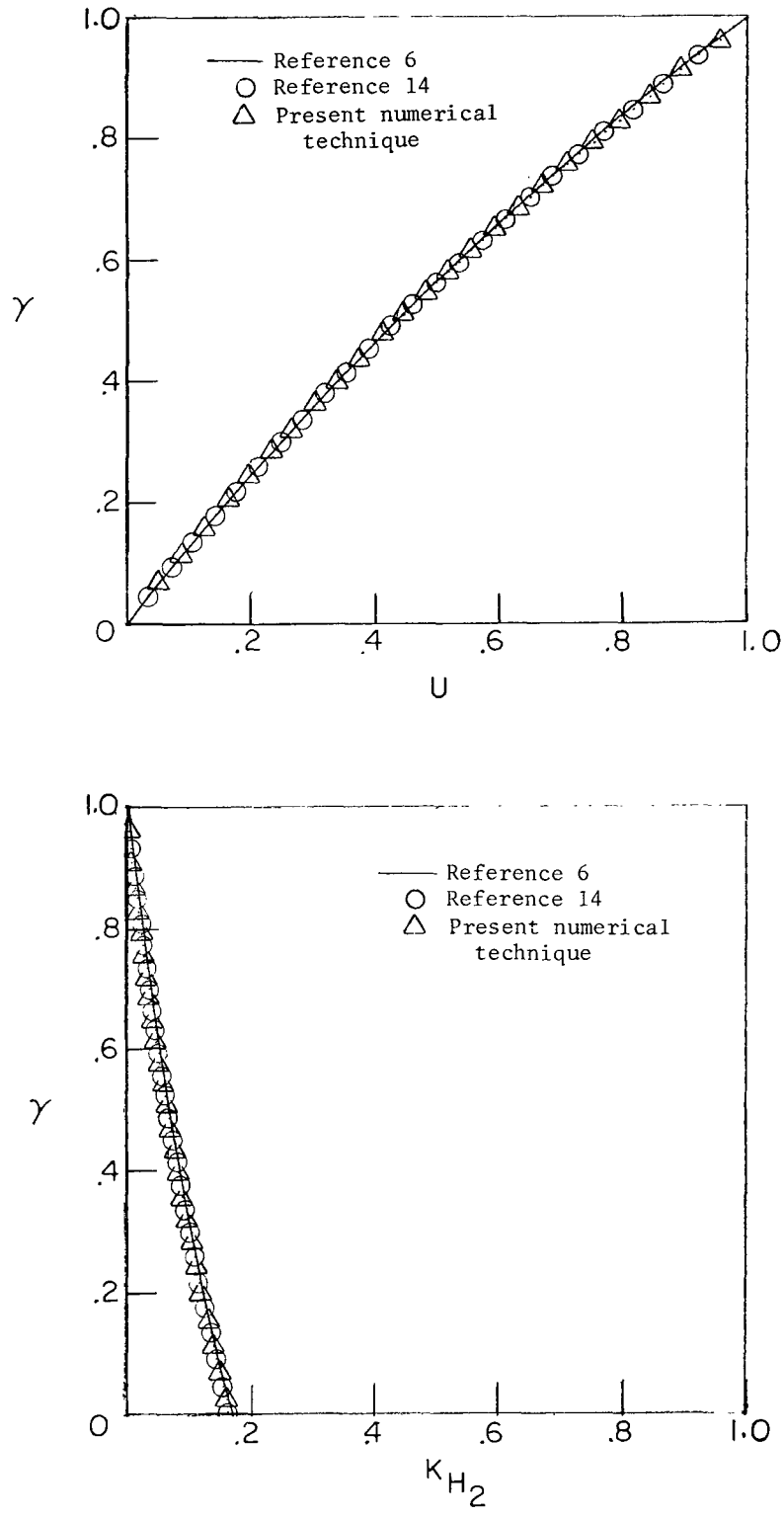

Figure 7.- Velocity and concentration profiles for nitrogen Couette flow with hydrogen injection.

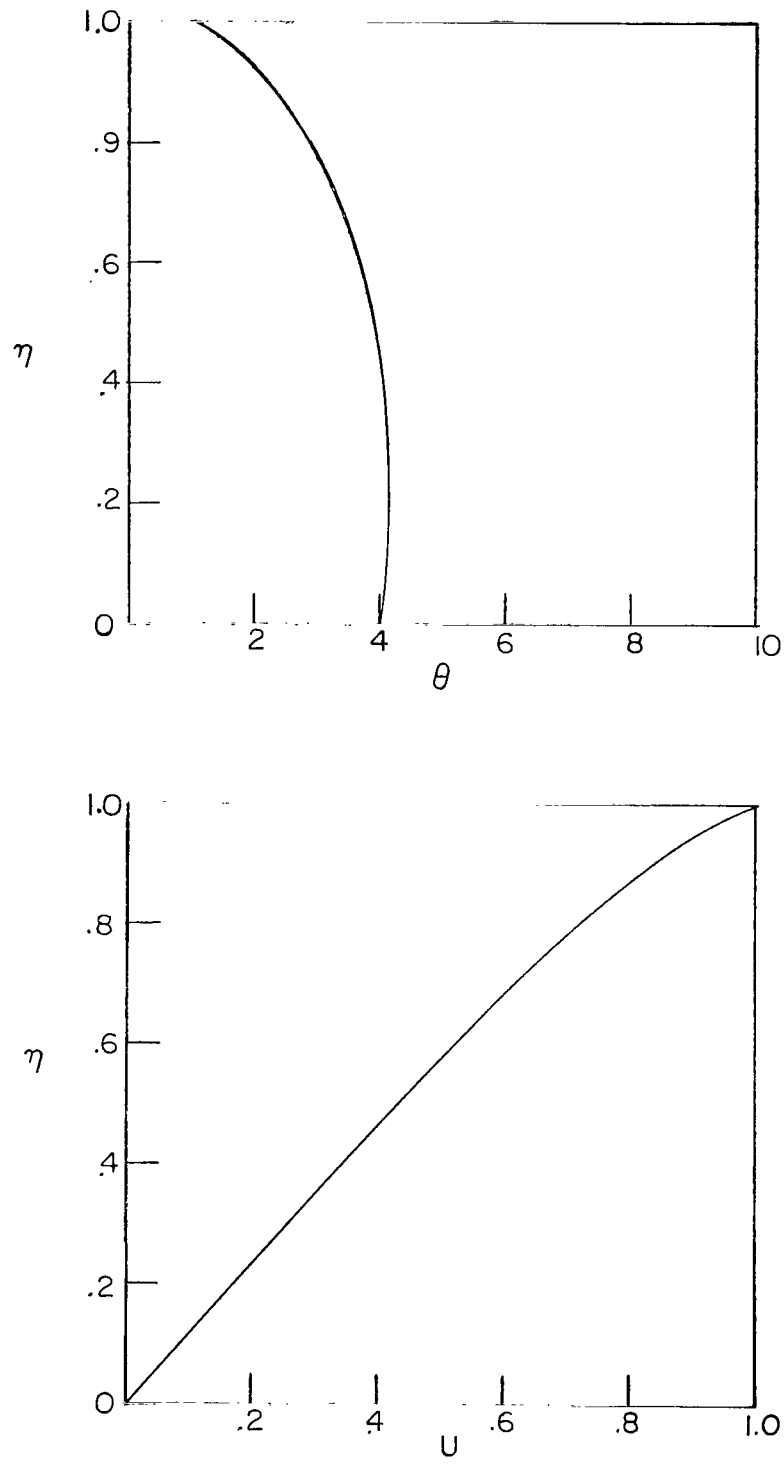

Figure 8.- No-injection temperature and velocity profiles.

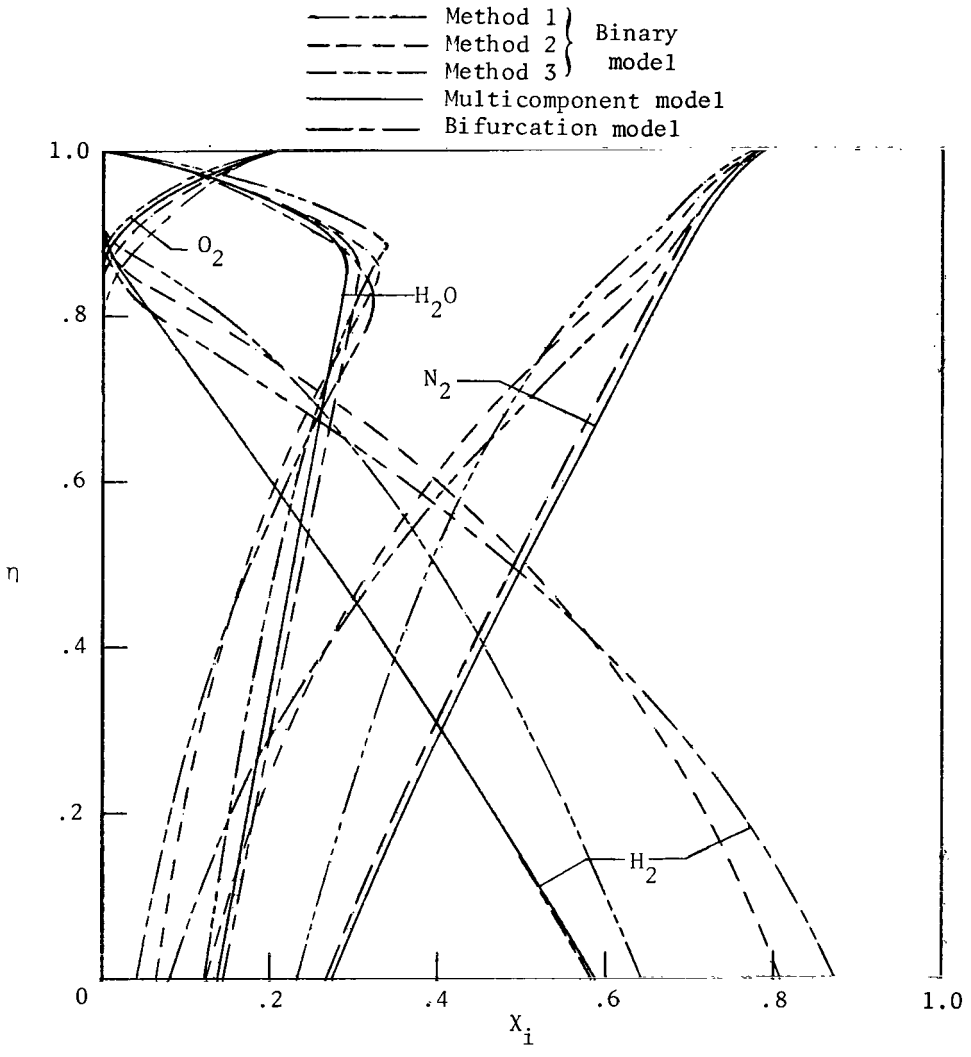

(a) $\delta = 1.3$.

Figure 9.- Concentration profiles.

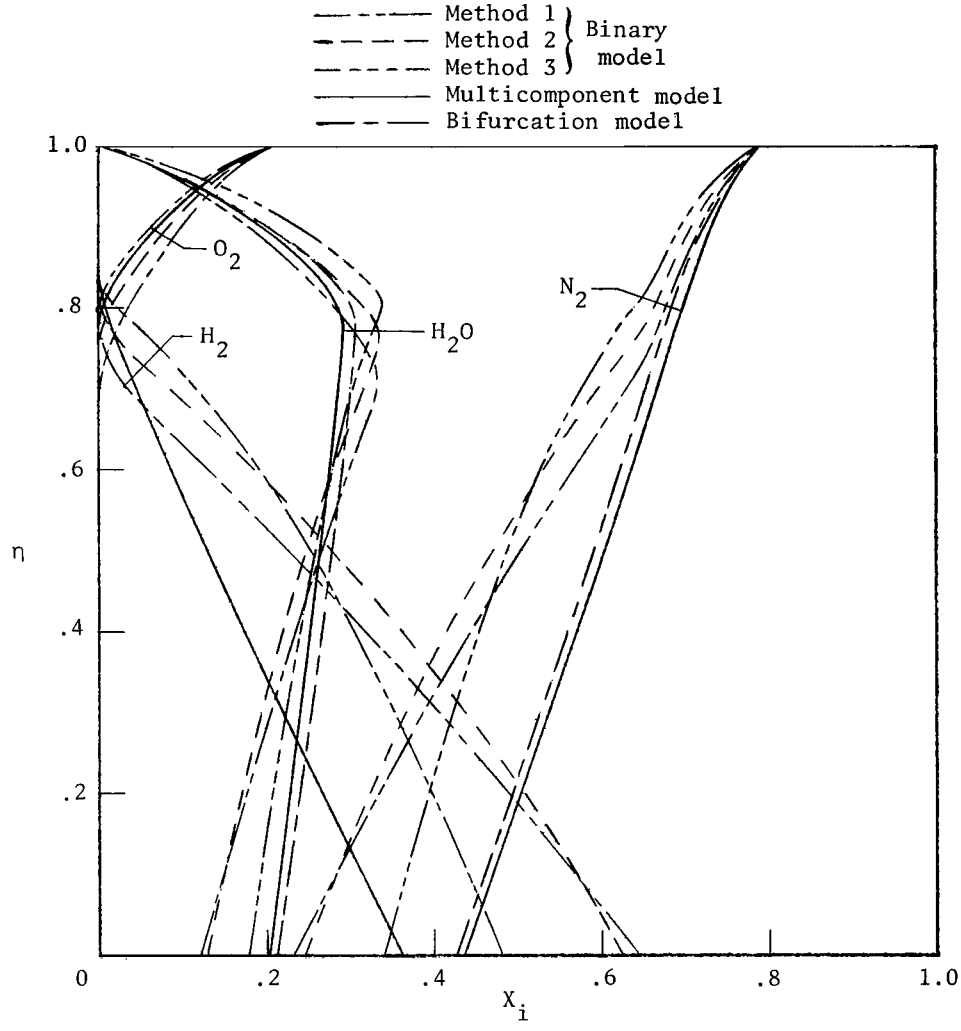

(b) $\delta = 0.75$.

Figure 9.- Continued.

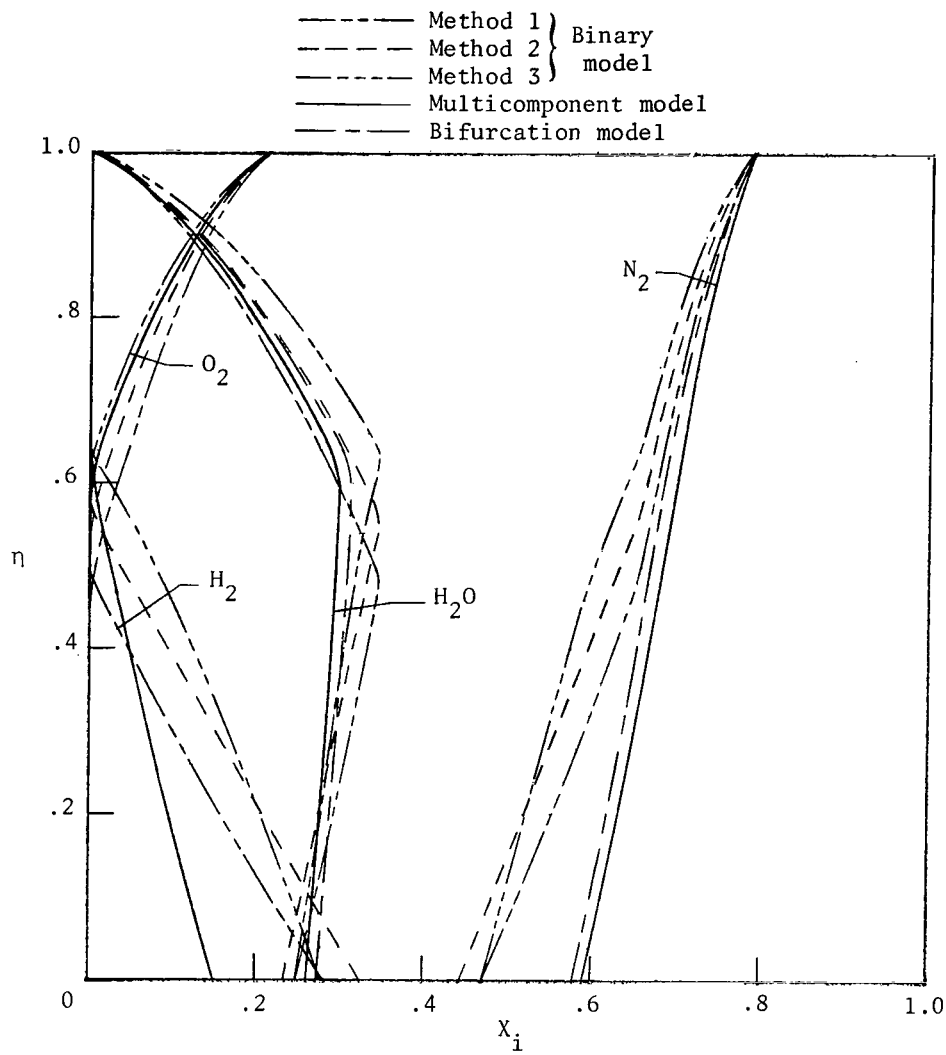

(c) $\delta = 0.35$.

Figure 9.- Continued.

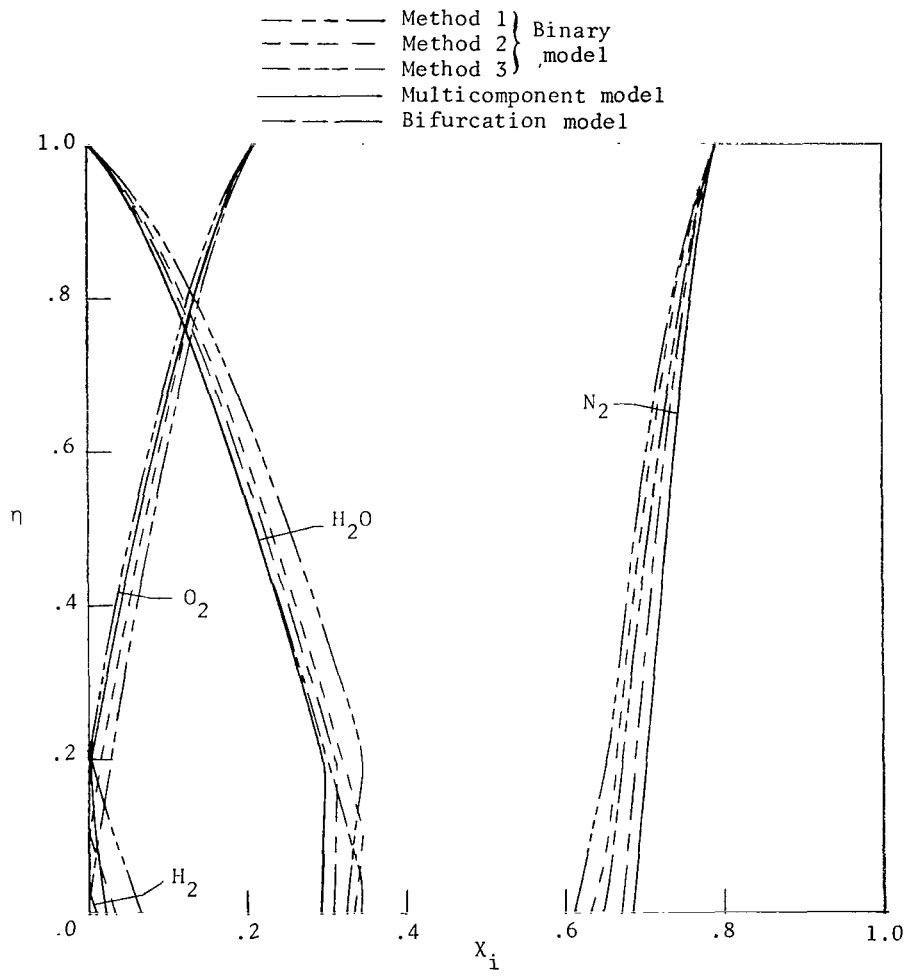

(d) $\delta = 0.13$.

Figure 9.- Concluded.

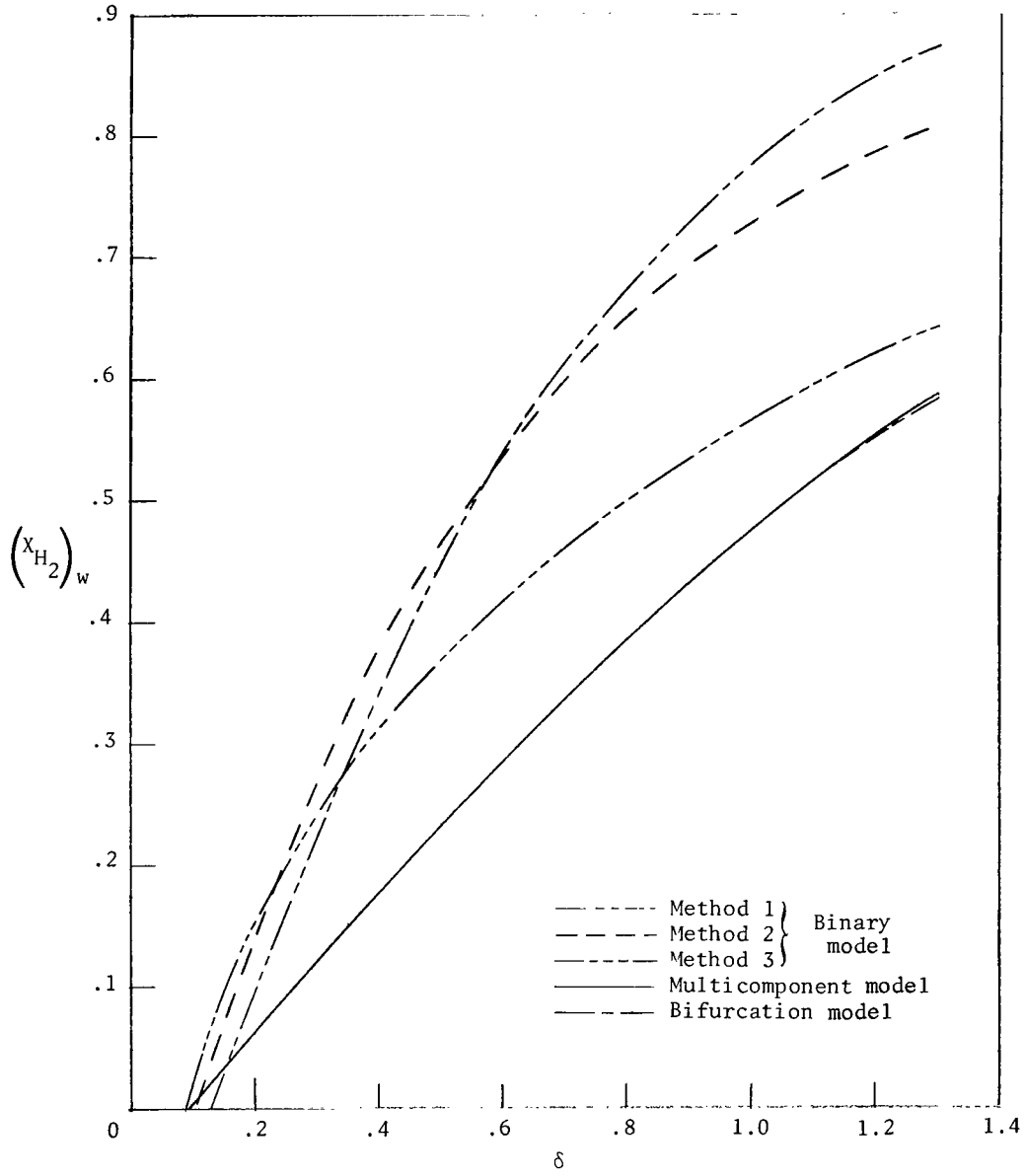

Figure 10.- Hydrogen concentration at the wall.

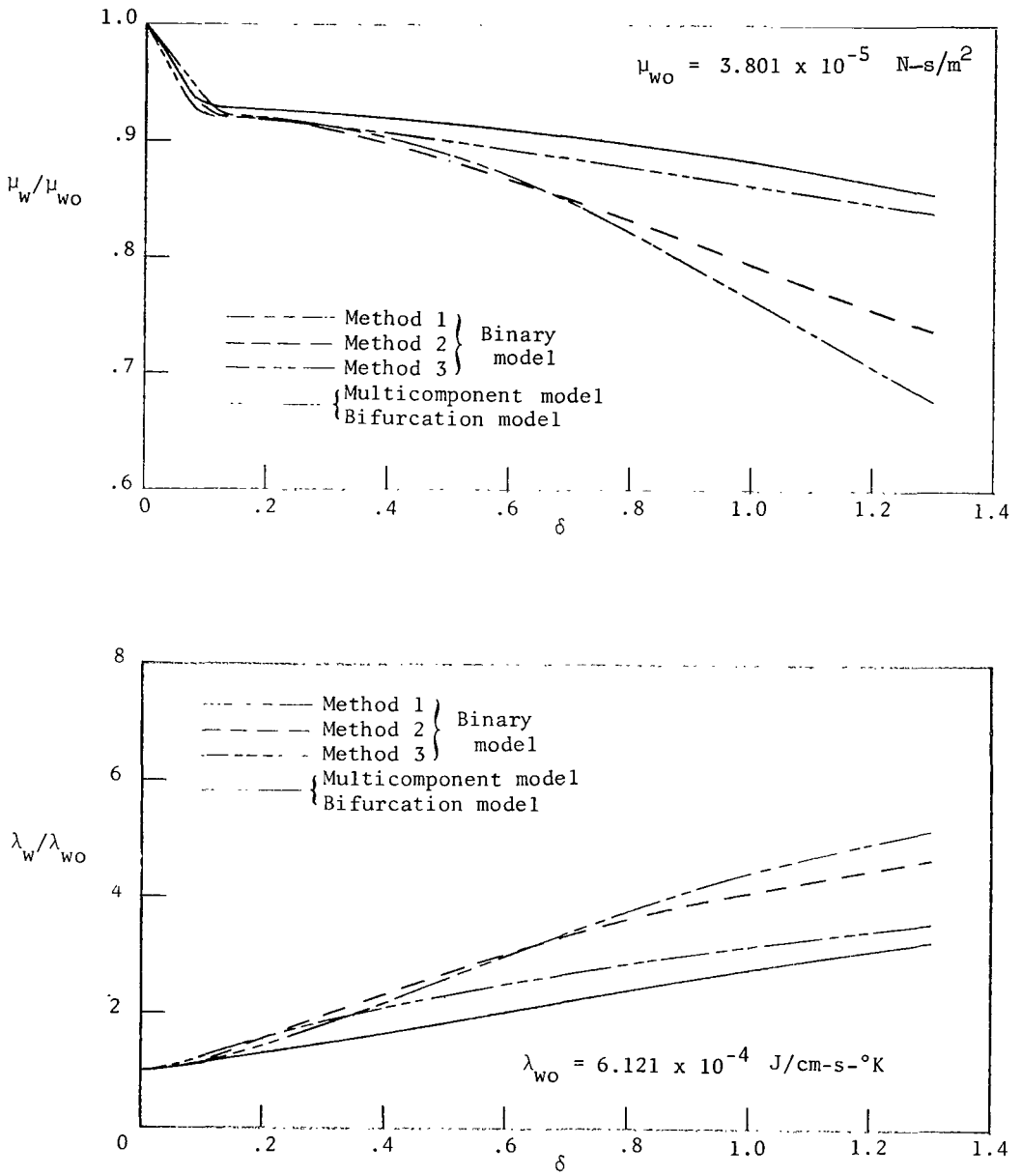

Figure 11.- Transport properties at the wall.

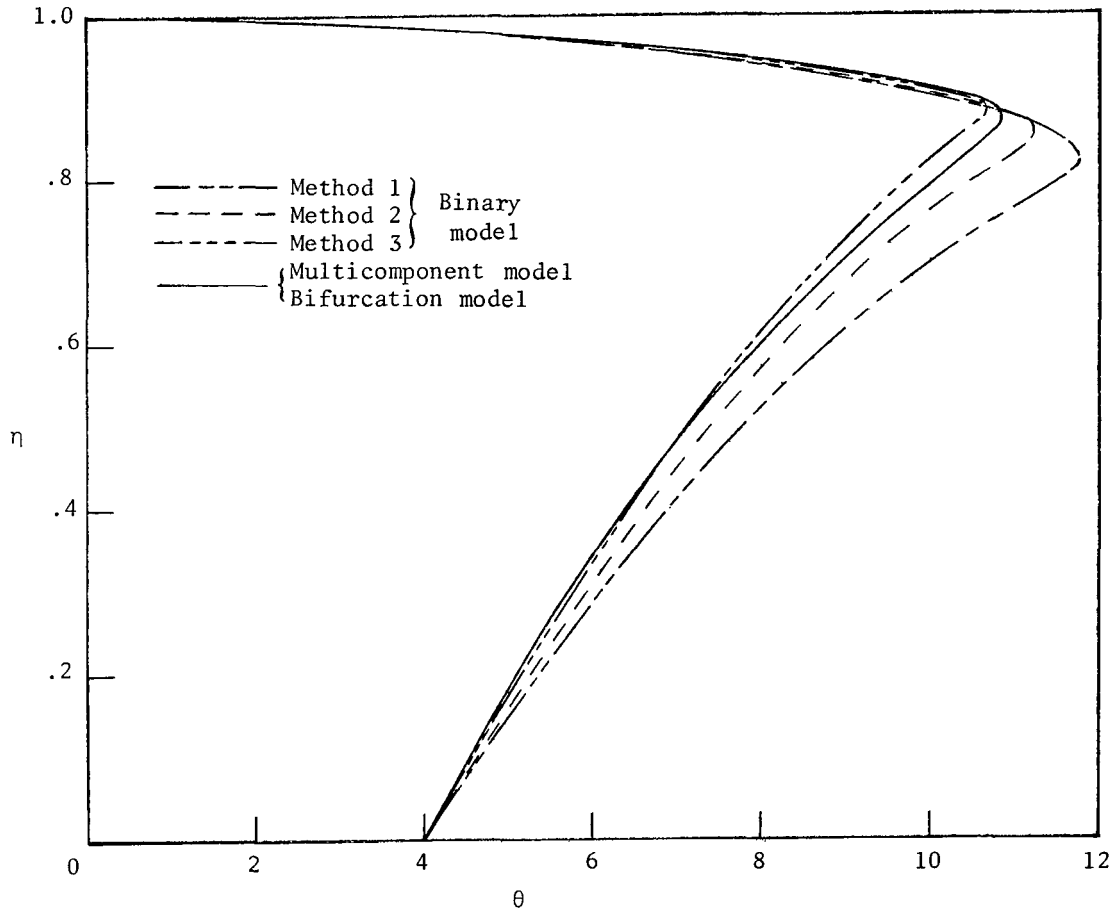

(a) $\delta = 1.3$.

Figure 12.- Temperature profiles.

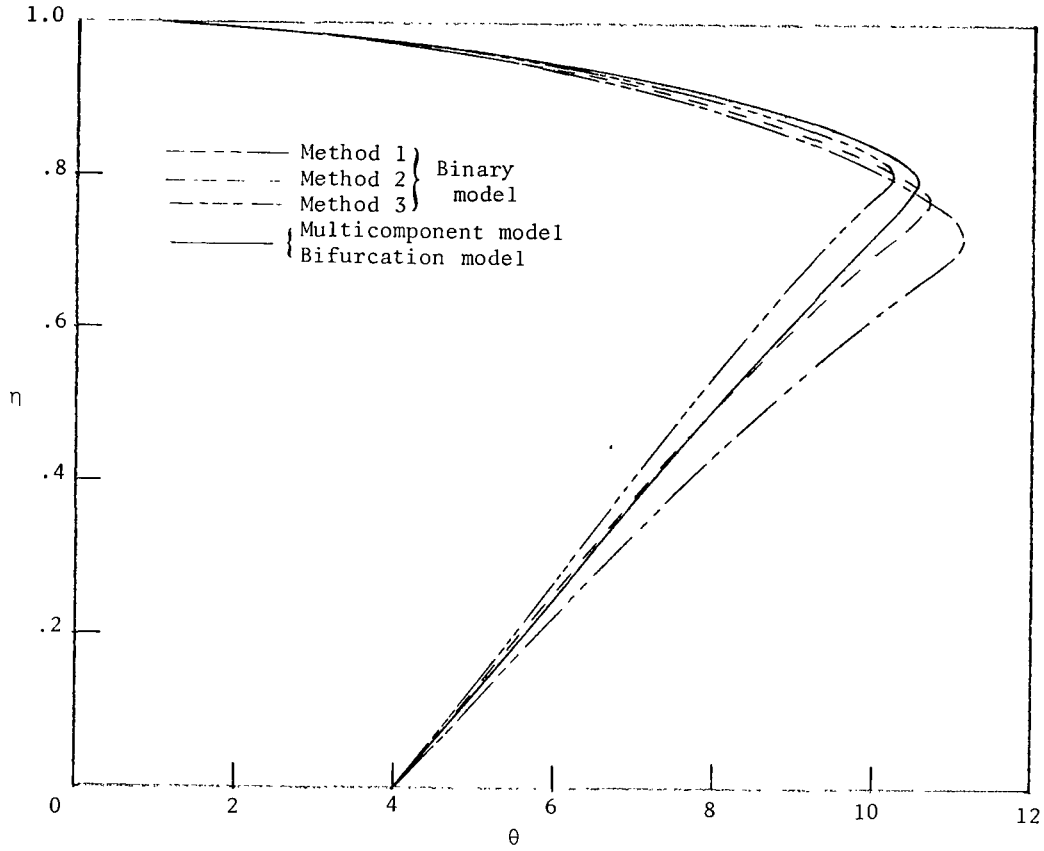

(b) $\delta = 0.75$.

Figure 12.- Continued.

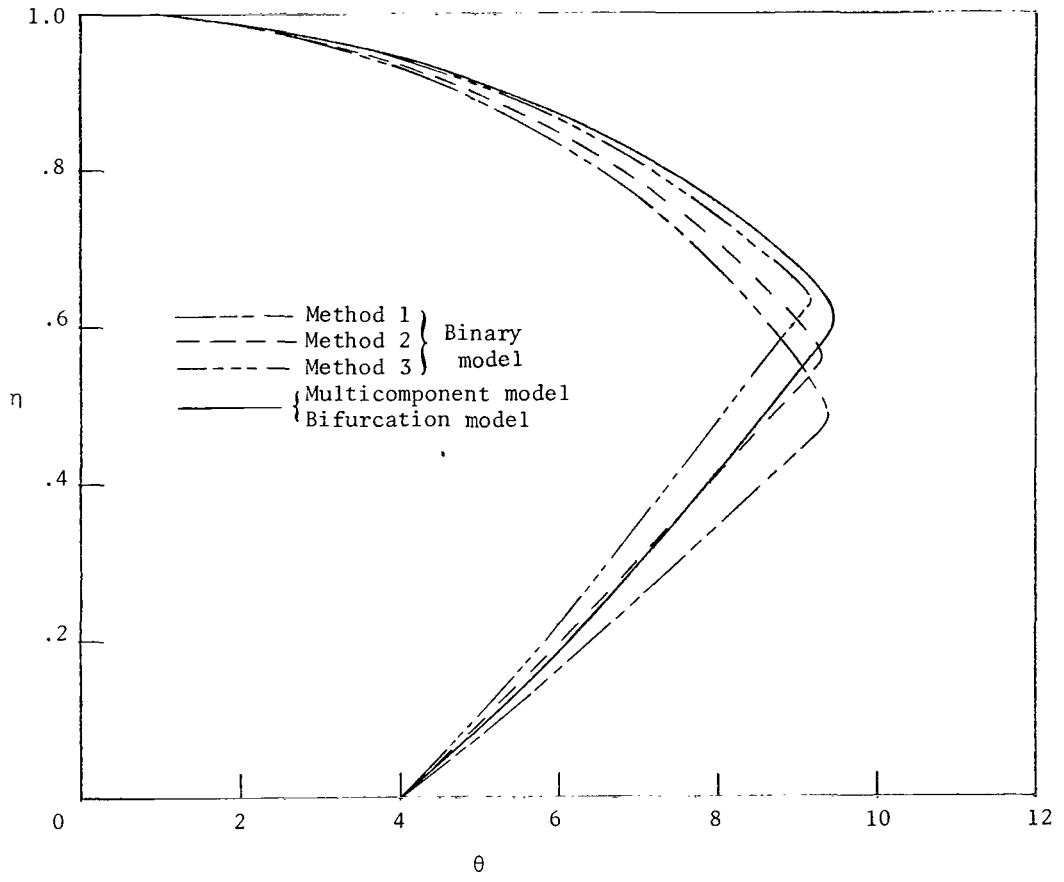

(c) $\delta = 0.35$.

Figure 12.- Continued.

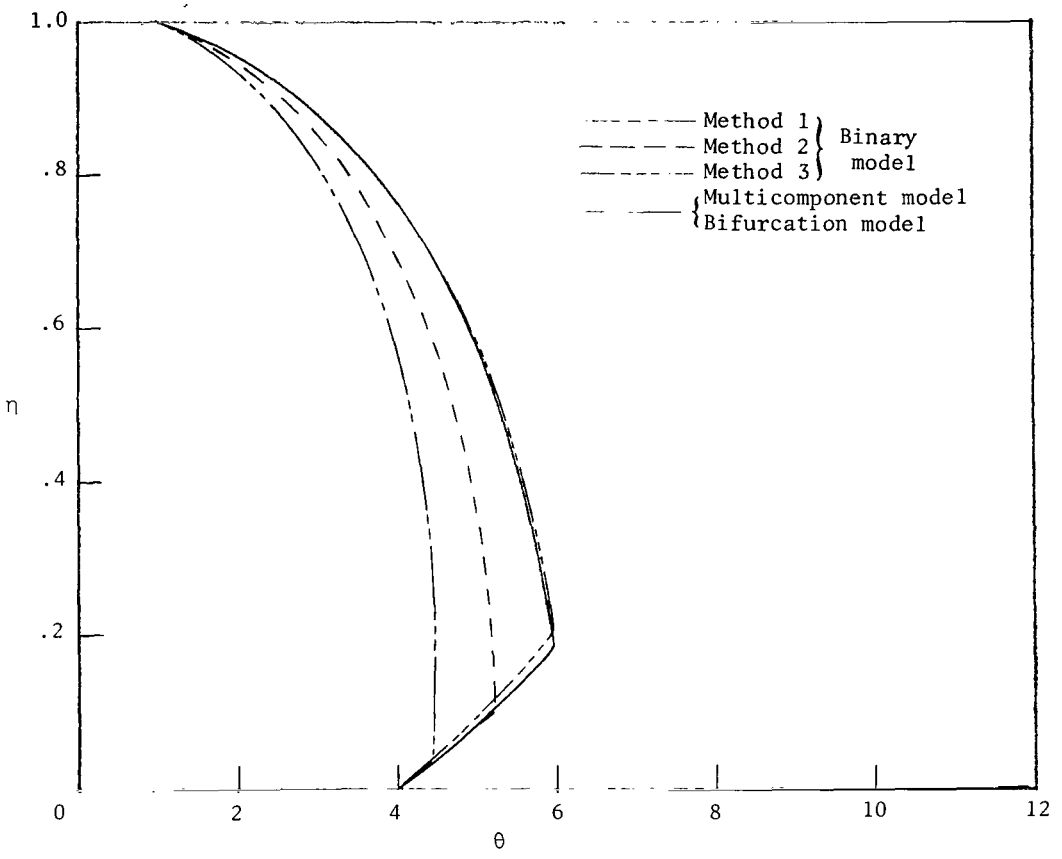

(d) $\delta = 0.13$.

Figure 12.- Concluded.

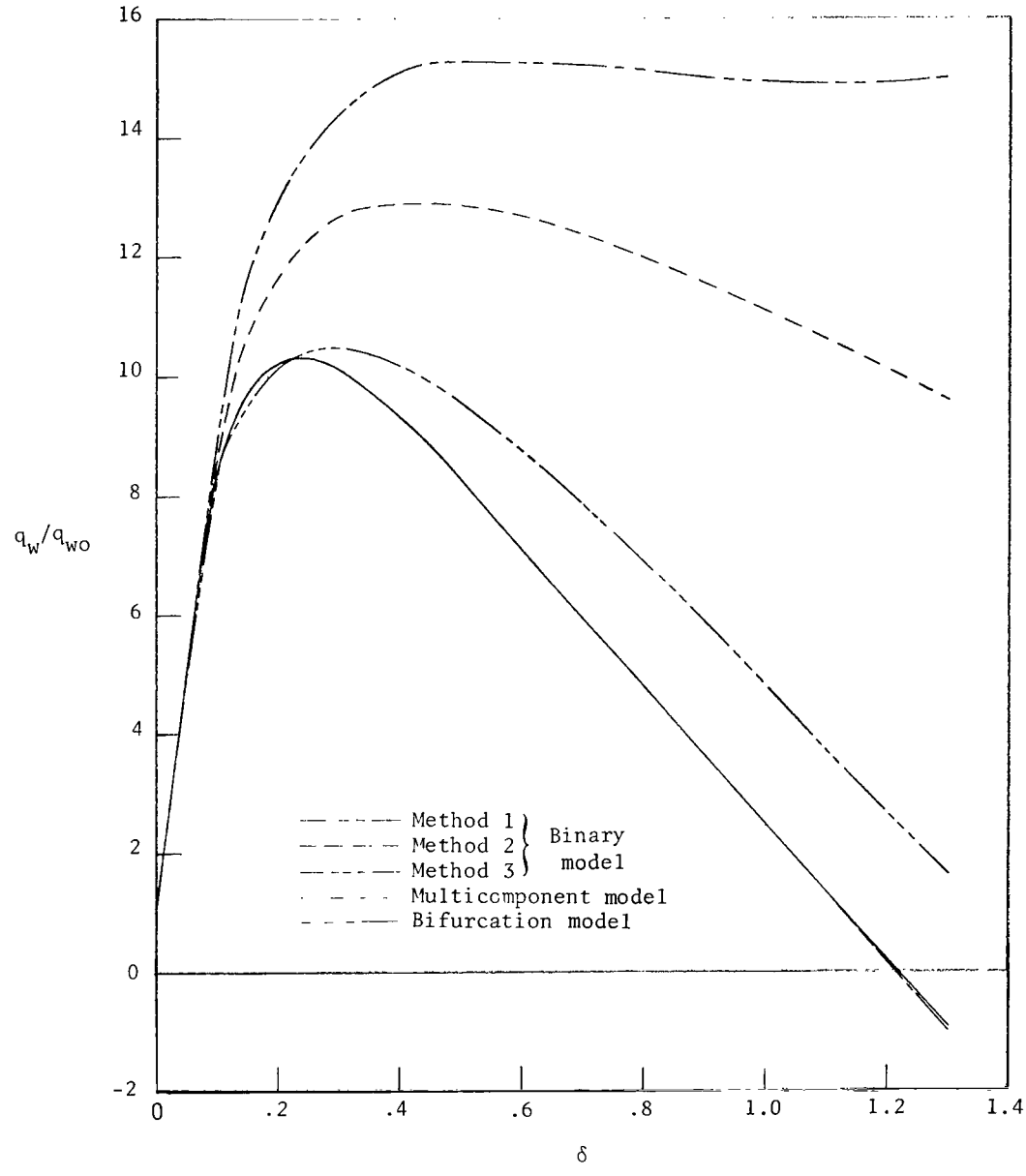

Figure 13.- Wall heating rates. $q_{wo} = 6.282$.

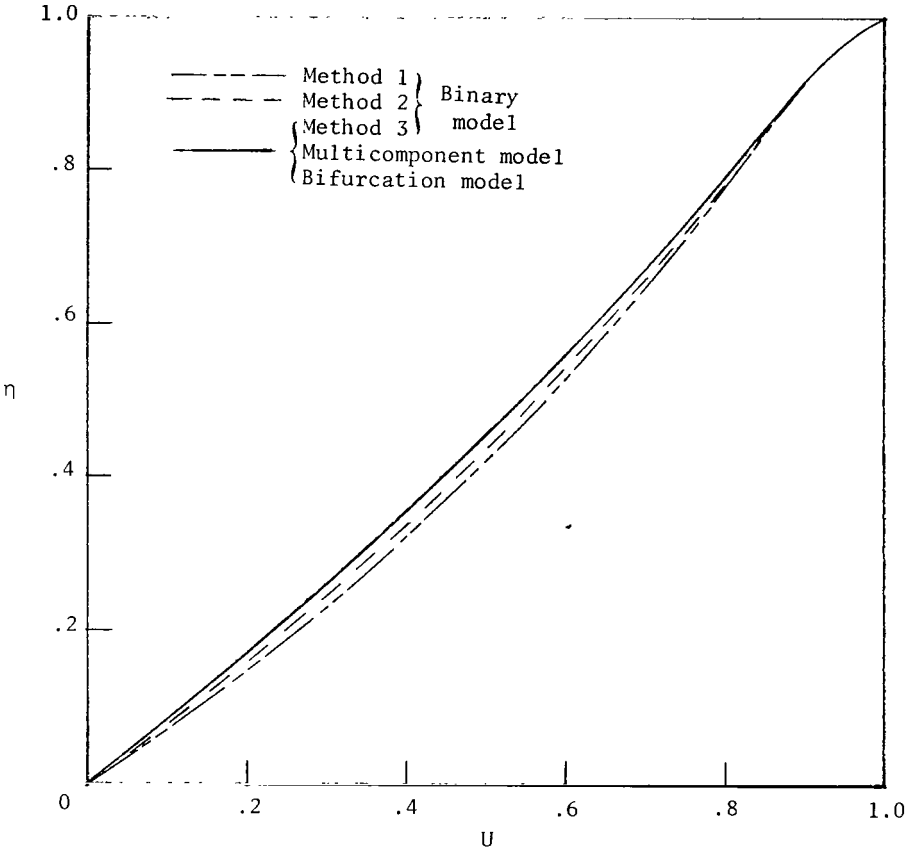

(a) $\delta = 1.3$.

Figure 14.- Velocity profiles.

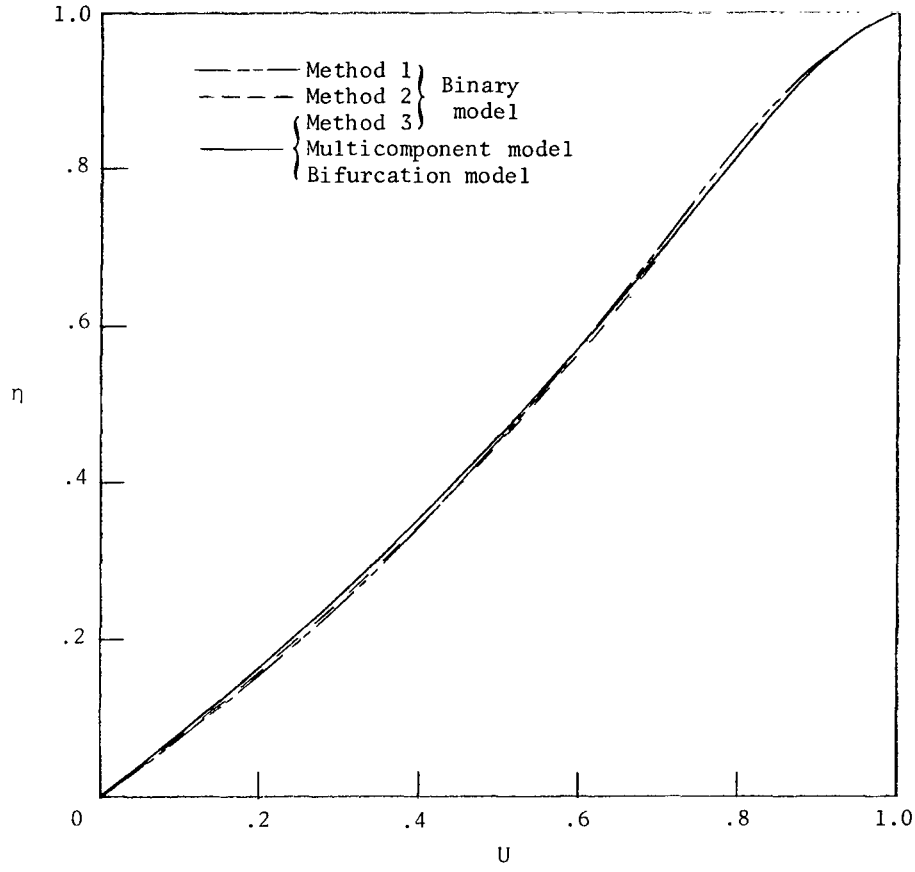

(b) $\delta = 0.75$.

Figure 14.- Continued.

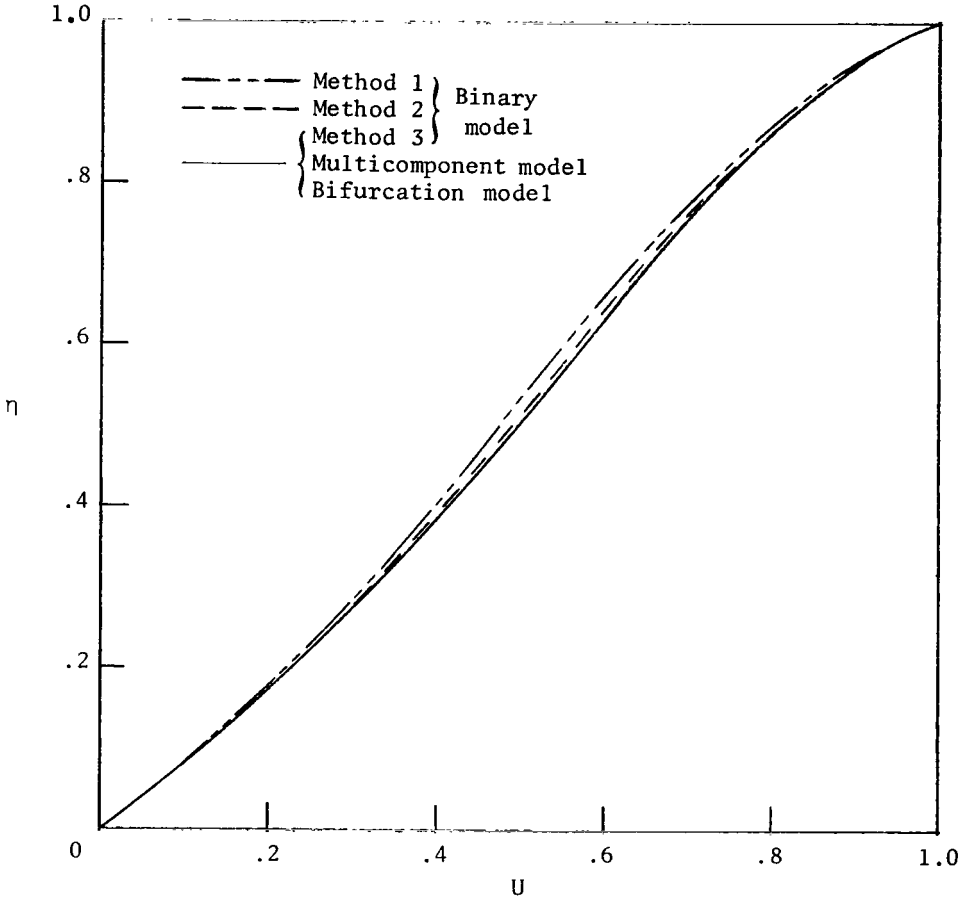

(c) $\delta = 0.35$.

Figure 14.- Continued.

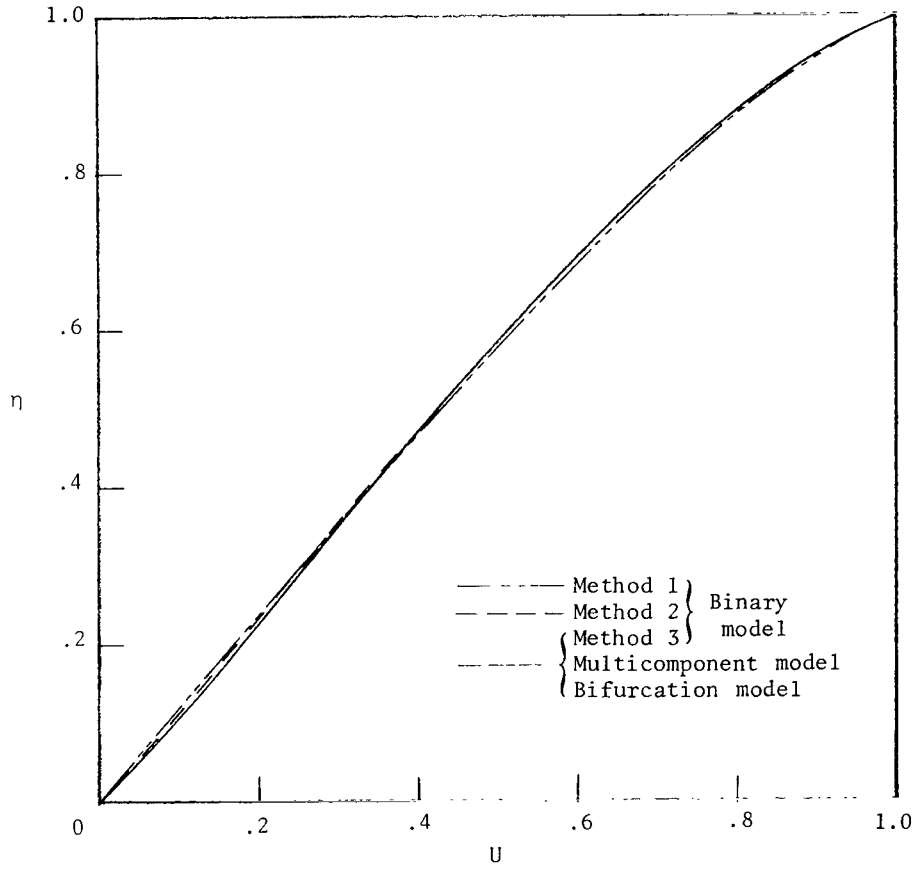

(d) $\delta = 0.13$.

Figure 14.- Concluded.

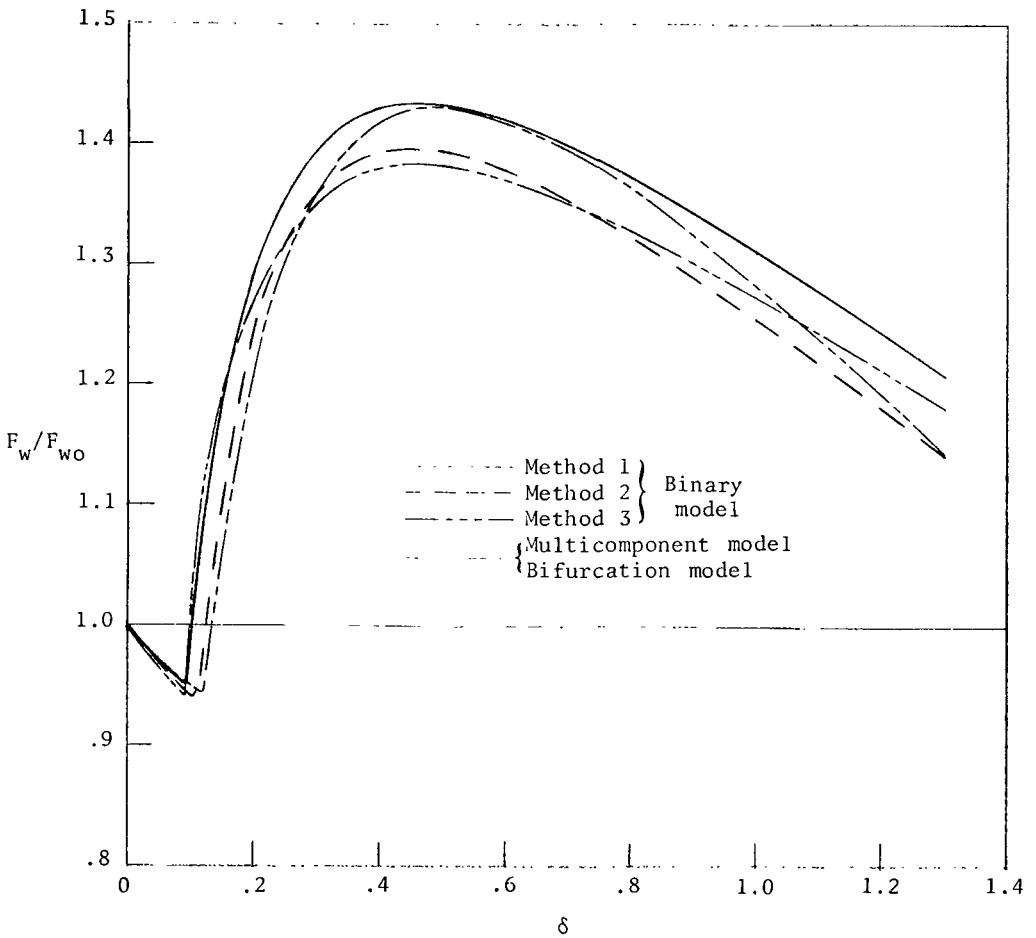

Figure 15.- Shear stress at the wall. $F_{wo} = 2.338$.

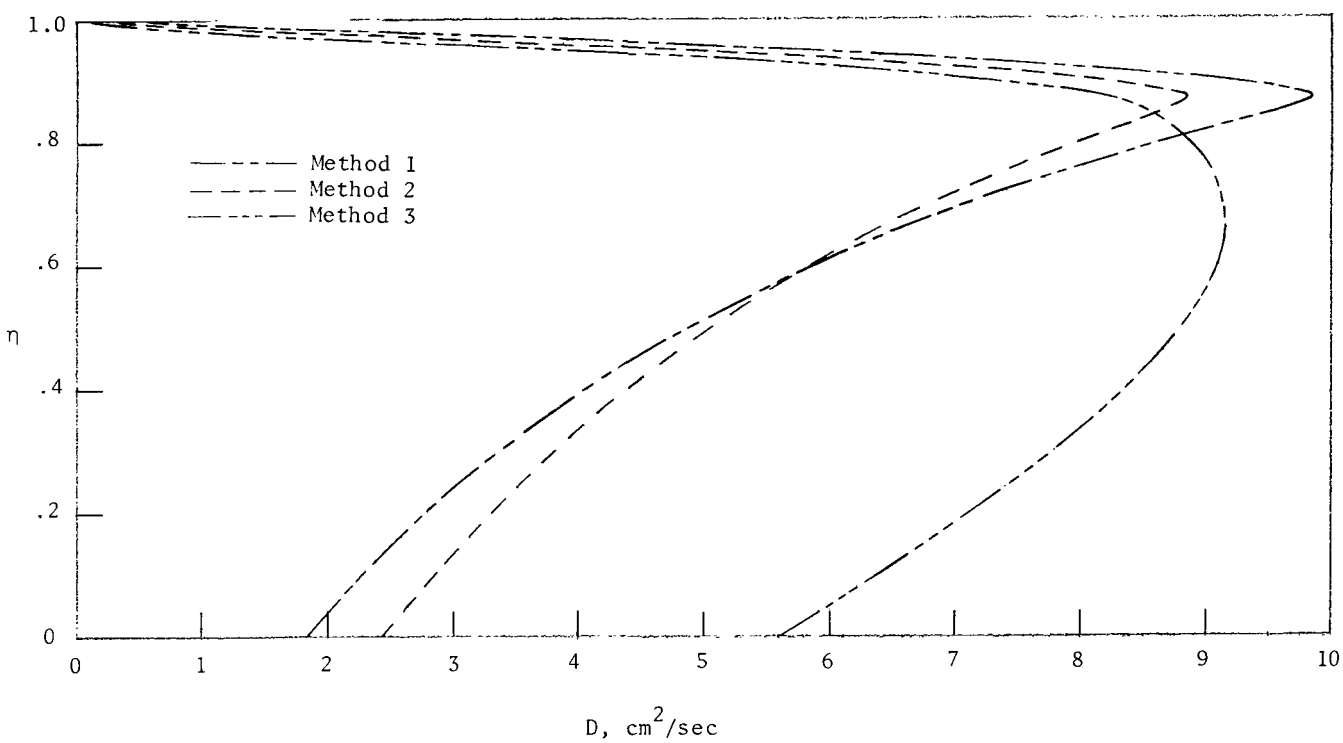

(a) $\delta = 1.3$.

Figure 16.- Fick's law diffusion coefficient profiles based on the temperature and concentration profiles of the multicomponent solution.

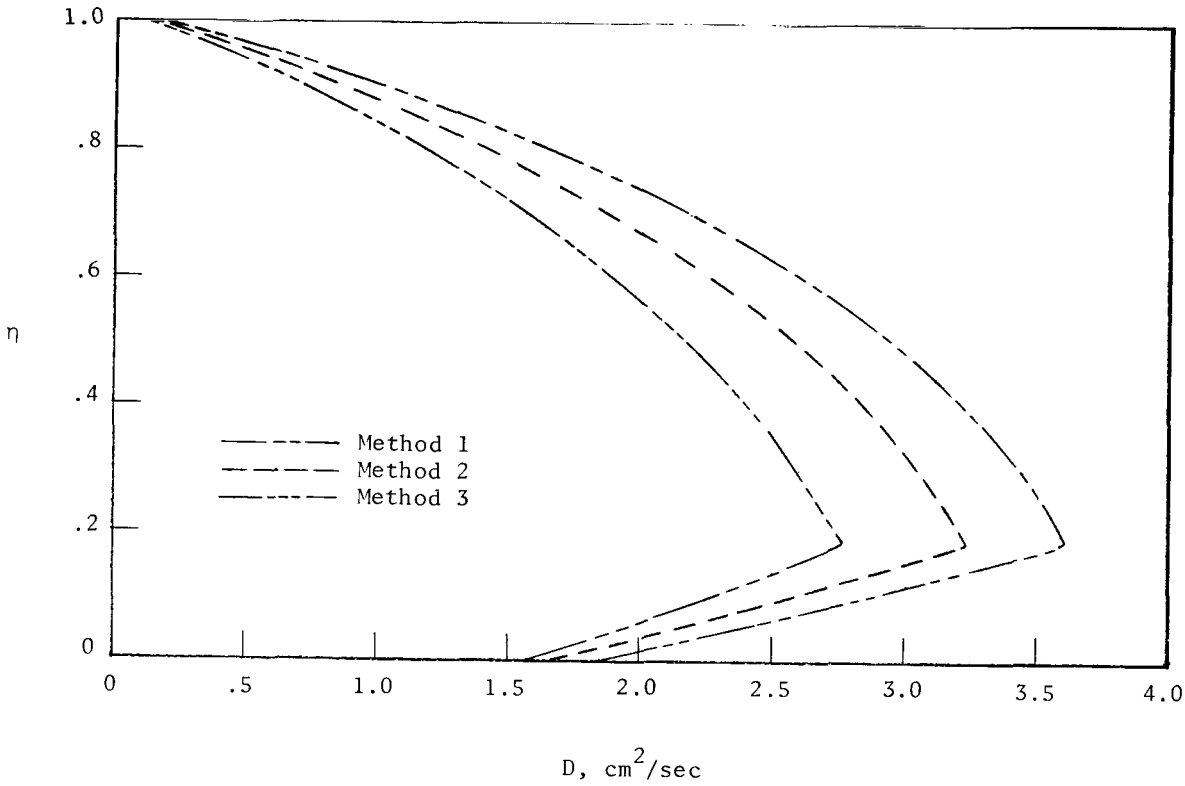

(b) $\delta = 0.13$.

Figure 16.- Concluded.

NASA-Langley, 1970 —— 33 L-6960

"The aeronautical and space activities of the United States shall be conducted so as to contribute . . . to the expansion of human knowledge of phenomena in the atmosphere and space. The Administration shall provide for the widest practicable and appropriate dissemination of information concerning its activities and the results thereof."

—NATIONAL AERONAUTICS AND SPACE ACT OF 1958

NASA SCIENTIFIC AND TECHNICAL PUBLICATIONS

TECHNICAL REPORTS: Scientific and technical information considered important, complete, and a lasting contribution to existing knowledge.

TECHNICAL NOTES: Information less broad in scope but nevertheless of importance as a contribution to existing knowledge.

TECHNICAL MEMORANDUMS: Information receiving limited distribution because of preliminary data, security classification, or other reasons.

CONTRACTOR REPORTS: Scientific and technical information generated under a NASA contract or grant and considered an important contribution to existing knowledge.

TECHNICAL TRANSLATIONS: Information published in a foreign language considered to merit NASA distribution in English.

SPECIAL PUBLICATIONS: Information derived from or of value to NASA activities. Publications include conference proceedings, monographs, data compilations, handbooks, sourcebooks, and special bibliographies.

TECHNOLOGY UTILIZATION PUBLICATIONS: Information on technology used by NASA that may be of particular interest in commercial and other non-aerospace applications. Publications include Tech Briefs, Technology Utilization Reports and Notes, and Technology Surveys.

Details on the availability of these publications may be obtained from:

SCIENTIFIC AND TECHNICAL INFORMATION DIVISION

NATIONAL AERONAUTICS AND SPACE ADMINISTRATION

Washington, D.C. 20546